International Journal of Nanomedicine

Dovepress
Taylor & Francis Group

Open Access Full Text Article

ORIGINAL RESEARCH

Physicochemical Stability and Cross-Context Validation of PEGylated Human Serum Albumin Nanoparticles for Dual Neurotrophin Delivery in the Rabbit Eye and Oxidative Stress Models

Iga Stukan[1,*], Maria Dąbkowska[2,*], Anna Machalińska[3], Karolina Łuczkowska[1], Kamila Pukacka[2], Monika Wasilewska[4], Patrycja Stodolak[1], Mateusz Winiarczyk[5], Dagmara Winiarczyk[6], Jowita Zwolska[7], Barbara Kuduk[7], Mateusz Szadkowski[7], Ireneusz Balicki[7], Miłosz Piotr Kawa[1], Bogusław Machaliński[1]

[1]Department of General Pathology, Pomeranian Medical University in Szczecin, Szczecin, Poland; [2]Department of Pharmacokinetics, Biopharmaceutics and Drug Delivery Systems, Pomeranian Medical University in Szczecin, Szczecin, Poland; [3]First Department of Ophthalmology, Pomeranian Medical University, Szczecin, Poland; [4]Jerzy Haber Institute of Catalysis and Surface Chemistry, Polish Academy of Sciences, Kraków, Poland; [5]Department of Vitreoretinal Surgery, Medical University of Lublin, Lublin, Poland; [6]Department of Internal Diseases of Small Animals, University of Life Sciences of Lublin, Lublin, Poland; [7]Department and Clinic of Animal Surgery, Faculty of Veterinary Medicine, University of Life Sciences in Lublin, Lublin, Poland

*These authors contributed equally to this work

Correspondence: Maria Dąbkowska, Department of Pharmacokinetics, Biopharmaceutics and Drug Delivery Systems, Pomeranian Medical University in Szczecin, Szczecin, Poland, Email maria.dabkowska@pum.edu.pl; Iga Stukan, Department of General Pathology, Pomeranian Medical University in Szczecin, Szczecin, Poland, Email iga.stukan@pum.edu.pl

Purpose: Neurotrophins such as brain-derived neurotrophic factor (BDNF) and neurotrophin-3 (NT3) exhibit pro-survival and homeostatic properties, but their clinical translation is limited by protein instability and rapid clearance. We evaluated a PEGylated human serum albumin (HSA) nanoparticle system for BDNF/NT3 co-delivery, focusing on physicochemical stability, ocular biodistribution in the rabbit eye, intracellular protein delivery, and protection against oxidative stress–associated cellular damage in human cells.

Materials and Methods: PEGylated HSA–BDNF–NT3 nanoparticles with nominal neurotrophin concentrations of 5 µg/mL (NeO5) or 10 µg/mL (NeO10) were generated by spontaneous self-assembly and characterized using multiangle dynamic light scattering, electrophoretic light scattering, and atomic force microscopy. In vivo performance was assessed after intravitreal injection in rabbits by enzyme-linked immunosorbent assay (ELISA)–based protein quantification and exploratory reverse transcription quantitative polymerase chain reaction (RT-qPCR) profiling of survival-, proliferation-, and apoptosis-related genes. Functional delivery was examined in sodium iodate-stressed ARPE-19 and 6-hydroxydopamine–stressed retinoic acid-differentiated SH-SY5Y cells using ELISA assays, JC-1 analysis, Annexin V/ propidium iodide flow cytometry, high-performance liquid chromatography for malondialdehyde quantification, and RT-qPCR.

Results: Both formulations formed stable, spherical nanoparticles (5.9–54.2 nm) with low polydispersity index (≈ 0.18) and preserved colloidal integrity over 28 days. In vivo, BDNF was detectable in ocular tissues up to 72 h and RT qPCR did not reveal a coordinated pro-apoptotic response under the tested conditions. In vitro, nanoparticle treatment significantly increased intracellular BDNF and NT3 levels, improved viability, reduced apoptotic cell fractions, and markedly decreased lipid peroxidation, particularly for NeO10. Increased tropomyosin receptor kinase B *TRKB* and cAMP response element-binding protein *CREB* expression provided supportive molecular evidence consistent with neurotrophin-related cellular responses.

Conclusion: PEGylated HSA nanoparticles enable stable neurotrophin loading, efficient intracellular delivery, and attenuation of oxidative stress–induced cytotoxicity. These findings support further development of albumin-based nanocarriers for translational nanomedicine applications.

Keywords: human serum albumin, PEGylated albumin nanoparticles, protein drug delivery, neurotrophin delivery, oxidative stress, drug delivery platform, nanomedicine, brain-derived neurotrophic factor, neurotrophin-3

https://doi.org/10.2147/IJN.S608949
Received: 19 March 2026
Accepted: 30 May 2026
Published: 30 June 2026

Introduction

Neurotrophins such as brain-derived neurotrophic factor (BDNF) and neurotrophin 3 (NT3) function as pleiotropic regulators of cellular homeostasis and stress resilience, yet their translation as protein therapeutics remains limited by physicochemical fragility, rapid clearance, and limited tissue bioavailability.[1–5] These barriers are particularly critical in the context of local delivery, where proteolysis, diffusion constraints, and compartment-specific barriers can rapidly reduce effective exposure despite high intrinsic potency. Accordingly, delivery strategies that stabilize neurotrophins and provide controlled, sustained availability while maintaining a favorable safety profile - are a prerequisite for meaningful therapeutic development. Although various strategies have been proposed for delivering BDNF alone,[6–12] the combined delivery of both BDNF and NT3 remains a relatively unexplored area. This combination holds significant potential due to the synergistic effects of NT3 in enhancing the therapeutic outcomes of BDNF through activation of additional receptors and pathways related to neuronal survival and synaptic plasticity.[13,14] Therefore, co-delivery of BDNF and NT3 may offer broader neurotrophin-related support than monotherapy. Human serum albumin (HSA) is an attractive carrier scaffold due to its biocompatibility and established use in drug delivery. Its surface chemistry enables adsorption-based loading of biologics.[15–18] Additionally, HSA facilitates active targeting of tissues via interactions with endothelial glycoproteins, such as gp60, which aid in tissue transcytosis.[17] Compared with PLGA nanoparticles, liposomes, polymeric micelles, or exosomes, PEGylated albumin-based carriers offer several advantages for the delivery of fragile therapeutic proteins.[17,19] Synthetic polymer systems often require harsh preparation conditions that may compromise neurotrophin stability, whereas liposomes and micelles may suffer from premature cargo leakage and limited colloidal stability.[20,21] Exosome-based systems, although biologically relevant, remain difficult to standardize and scale up. In contrast, albumin is an endogenous, biocompatible protein with low immunogenicity, prolonged circulation half-life, and intrinsic ligand-binding capacity. Moreover, albumin nanoparticles can be assembled under mild aqueous conditions that better preserve the biological activity of sensitive proteins.[22]

In our previous work, we introduced a straightforward, nonviral PEGylated HSA nanoparticle system engineered for co-delivery of BDNF and NT3, and demonstrated favorable electrokinetic properties, in vitro biocompatibility, and gradual neurotrophin release over extended timeframes in both cell-free conditions and the mouse eye following intravitreal injection. Notably, the prior study emphasized the platform's capacity for sustained intraocular availability and provided a proof-of-concept foundation for subsequent translational evaluation.[16]

Here, we assess robustness of the platform across biological contexts that are critical for translational development, including interspecies performance and stress-relevant cellular models. Specifically, we (i) characterize PEGylated HSA–BDNF-NT3 nanoparticles (NeO5 and NeO10) with respect to stability and physicochemical properties over time, (ii) assess intraocular biodistribution and early transcriptional responses following intravitreal administration in the rabbit eye, and (iii) validate functional delivery under oxidative stress in two human cell systems: sodium iodate ($NaIO_3$)-challenged ARPE-19 cells, representing retinal pigment epithelium oxidative injury relevant to AMD-associated pathology,[23,24] and 6-hydroxydopamine (6-OHDA)-challenged retinoic acid (RA)-differentiated SH-SY5Y cells, representing a neuronal oxidative stress model commonly used in Parkinsonian neurodegeneration research.[25,26] Across these settings, we quantify cellular uptake of both the carrier and its cargo, interrogate neurotrophin-related signaling, and assess apoptosis- and oxidative stress–related response to determine whether PEGylated albumin nanoparticles preserve neurotrophin functionality and provide measurable cytoprotection under defined stress conditions (Figure 1).

Materials and Methods

Reagents

BDNF, NT3 and HSA

Carrier-free recombinant human BDNF (248-N4-250/CF; R&D Systems, MN, USA) and carrier-free recombinant human NT3 (11563-N3; R&D Systems, MN, USA) lyophilizates were prepared as described in our previous studies.[16,27] The source of HSA used as a carrier for NTs' adsorption was Flexbumin (95% human albumin, 200 g/L, sodium chloride, sodium caprylate, sodium acetyltryptophanate and water).[16]

According to the manufacturer's quality control documentation, endotoxin levels for recombinant BDNF and NT3 were <0.10 EU per 1 μg of protein, as determined by the LAL method.

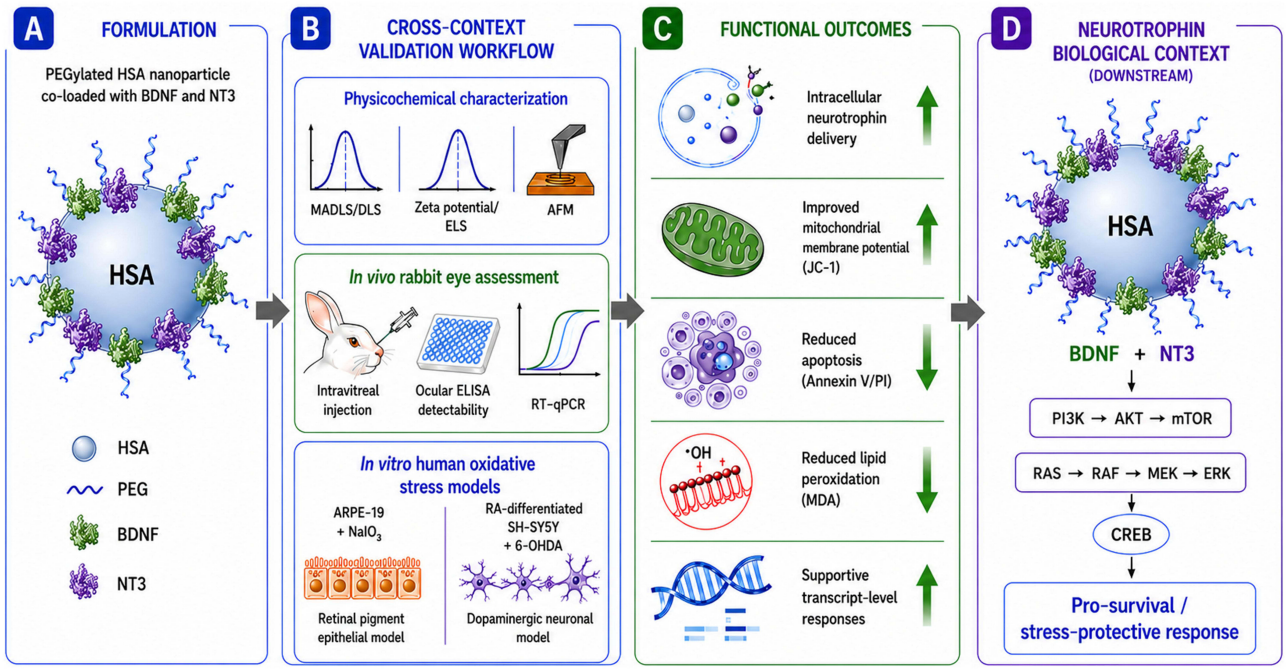

Figure 1 Cross-context biological validation of PEGylated HSA nanoparticles co-loaded with BDNF and NT3. Schematic overview of the study workflow and key biological findings. (**A**) PEGylated human serum albumin (HSA) nanoparticles were formulated for dual delivery of BDNF and NT3. (**B**) Cross-context validation included physicochemical characterization (MADLS/DLS, zeta potential/ELS, AFM), in vivo rabbit eye assessment following intravitreal administration, and in vitro oxidative stress models using ARPE-19 retinal pigment epithelial cells and RA-differentiated SH-SY5Y dopaminergic-like neurons. (**C**) Functional analyses demonstrated intracellular neurotrophin delivery associated with improved mitochondrial membrane potential, reduced apoptosis, decreased lipid peroxidation, and supportive transcript-level responses under oxidative stress conditions. (**D**) The downstream panel highlights canonical PI3K/AKT/mTOR and RAS/RAF/MEK/ERK signaling axes induced by NT3/BDNF that may contribute to CREB-associated stress-protective responses. The schematic illustrates a conceptual downstream signaling framework and does not imply a specific receptor-mediated nanoparticle uptake mechanism. Conceptual workflow illustration created with assistance from ChatGPT (OpenAI, GPT-5 image generation tools) and finalized by the authors.

Poly (Ethylene Glycol) (PEG)

The working solution of PEG (1546569, Sigma Aldrich, Darmstadt, Germany) was prepared by aseptically dissolving 1 g of PEG-4000 in 10 mL of PBS, filtered through a 0.22 μm filter (Merck Millipore, MA, USA), and was further used in the preparation of PEGylated HSA-NT3-BDNF nanoparticles.[16,27]

Preparation of PEGylated HSA/NT3/BDNF (NeO5, NeO10 and NeO100)

The detailed formulation procedure has been described previously.[16] However, all nanoparticle formulations used in the present study were synthesized de novo as independent batches specifically prepared for the current in vitro and in vivo experiments. In contrast to our previous work, where physicochemical characterization was performed primarily for a single formulation containing 5 μg/mL neurotrophins, the present study included three independently prepared nanoparticle formulations differing in neurotrophin loading: NeO5, NeO10, and NeO100, corresponding to 5, 10, and 100 μg/mL of NT3 and BDNF, respectively. Importantly, the physicochemical parameters obtained for NeO10 and NeO100, including hydrodynamic diameter, zeta potential, and colloidal stability, remained consistent with those previously observed for NeO5, confirming preservation of the overall physicochemical behavior of the PEGylated HSA-based nanoparticle system across the tested loading range. Briefly, Flexbumin was diluted in Ringer's solution by gentle rotation to obtain an HSA concentration of 200 mg/L. NT3 and BDNF stock solutions were added sequentially at defined volumetric ratios to obtain NeO5, NeO10, and NeO100 formulations, corresponding to nominal final concentrations of 5, 10, and 100 μg/mL, respectively, for each neurotrophin. These nominal values refer to the total amount of BDNF and NT3 introduced during preparation, not to the freely soluble protein fraction, as the neurotrophins are associated with the PEG/HSA nanoparticle system and released over time. Finally, PEG-4000 was added to a final concentration of 2 mg/L. Spontaneous self-assembly of PEG/HSA/NT3/BDNF complexes occurred through intermolecular and electrostatic

https://doi.org/10.2147/IJN.S608949

interactions, yielding formulations referred to as NeO5, NeO10, and NeO100. All formulations underwent independent physicochemical characterization, including hydrodynamic diameter and zeta potential measurements, to validate the properties of the newly synthesized nanoparticle batches used in the present study. The nanoparticle suspensions were stored in Ringer's solution at −20°C for up to three months without detectable protein loss.[16]

Physicochemical Characterization of PEGylated HSA/NT3/BDNF Nanoparticles

Multiangle Dynamic Light Scattering (MADLS)

The size distribution of PEGylated HSA/BDNF/NT3 nanoparticles was examined using multiangle dynamic light scattering (MADLS) with a Malvern ZetaSizer Ultra (Malvern Instruments, Malvern, UK) and ZS XPLORER 3.2.0 software. Both MADLS and dynamic light scattering (DLS) are well-established methods for assessing the hydrodynamic diameter distribution of biomacromolecules in solution, with MADLS being particularly effective for analyzing nanoparticle dispersion and aggregation states. Particle size distributions were measured at BDNF/NT3 concentrations of 5 mg/L and 10 mg/L.[28,29] The data analysis was performed in automatic mode at 25 °C using Ringer's solution as the dispersant medium, with a viscosity of 0.8872 mPa·s and a refractive index of 1.33. The measured nanoparticle diameter (d_H) is presented as the average value of 20 runs, with triplicate measurements within each run, as described in detail elsewhere.[29,30]

Electrophoretic Light Scattering (ELS)

The zeta potential (ζ) and polydispersity index (PDI) of the nanoparticles were studied using laser Doppler velocimetry (LDV) at 25 °C with a Malvern ZetaSizer Ultra Particle Analyzer, based on diffusion coefficient and electrophoretic mobility measurements. The LDV technique, as described by Adamczyk et al, relies on detecting changes in microphoretic mobility during the adsorption of the analyzed proteins or particles onto a model colloidal particle.[31] The electrophoretic mobility was recalculated to the ζ-potential using the Henry equation, which is valid for higher ionic strengths in which the polarization of the electric double layer is relevant (the double-layer thickness decreases relative to the protein dimension).

Atomic Force Microscopy (AFM)

The AFM experiments were performed as follows. Freshly cleaved mica sheets were immersed in PEGylated HSA/BDNF/NT3 nanoparticle suspensions (NeO10 NPs) prepared in 0.15 M Ringer's solution at a protein concentration of 10 mg/L (BDNF and NT3). The mica sheets were incubated in the nanoparticle suspension for 1 min at 298 K under diffusion-controlled conditions in a thermostated environment, allowing controlled adsorption of nanoparticles onto the mica surface without prior surface modification. After incubation, each sample was thoroughly rinsed with ultrapure water to remove residual solutes and loosely bound material, preventing crystallization artifacts. The samples were then air-dried overnight. The selected nanoparticle concentration was based on prior physicochemical characterization, ensuring appropriate dispersion and minimizing aggregation to obtain uniform, non-overlapping surface coverage suitable for quantitative analysis. The mica substrates with adsorbed PEGylated HSA/BDNF/NT3 nanoparticles were visualized by AFM to determine nanoparticle morphology and size distribution. Imaging was performed in air using an NT-MDT Solver microscope equipped with a SMENA-B scanning head. Measurements were carried out in semi-contact mode using high-resolution silicon probes (polysilicon cantilevers ETALON) with resonance frequencies of 77–114 kHz (±10%). The typical tip cone angle was below 20°. Images were recorded at a scan rate of 1 Hz over scan areas ranging from 0.5 μm × 0.5 μm to 20 μm × 20 μm, covering 10–20 randomly selected regions of each mica sheet. The relative measurement precision was estimated at 5%. All experiments were conducted at a stable temperature of 298 K. Image flattening was performed using the algorithm provided with the instrument. The presented micrographs represent direct surface detection without coating or additional modification. The size of the PEGylated HSA/BDNF/NT3 nanoparticles was determined using ImageJ software (https://imagej.net/ij/index.html) by gathering the number and coordinates of a minimum of 300 nanoparticles. The counting of PEGylated HSA/BDNF/NT3 nanoparticle dimensions involved a manual process that involved comparing the initial image and a modified version obtained through digital image filters. Specifically, altering the picture's background was instrumental in this method. By applying these filters, we assessed the accuracy of the particle analysis using the software mentioned above.

Cell Culture

Unless indicated otherwise, all reagents were purchased from Gibco (Thermo Fisher Scientific, Waltham, MA, USA). All cell lines were kept in a cell culture incubator (Thermo Fisher Scientific, Waltham, MA, USA) at a constant 37 °C and a humidified atmosphere consisting of 95% air and 5% CO_2. All cell cultures were routinely tested for mycoplasma contamination with LookOut® Mycoplasma qPCR Detection Kit (MP0040A, Sigma-Aldrich, Darmstadt, Germany) and were confirmed to be mycoplasma-negative before experiments.

Light microscopy images were acquired using a Zeiss Axio Vert.A1 microscope, equipped with Axiocam 105, and image analysis was performed with Zen 2.3 (blue edition) software (all from Carl Zeiss Microscopy, GmbH, 2011) and Fiji (ImageJ 1.54g).

The selected stressor concentrations of 6-OHDA and $NaIO_3$ were based on preliminary dose–response experiments (Supplementary Figure 1) and were consistent with concentrations previously used to induce oxidative injury in ARPE-19/RPE and differentiated SH-SY5Y models.

Arpe-19

The human retinal pigment epithelial line ARPE-19 (CRL-2302™ ATCC®, Manassas, VA, USA) was cultured in DMEM/F12 medium with the addition of 1% (*v/v*) penicillin/streptomycin and 10% (*v/v*) fetal bovine serum (FBS). For experiments, cells were seeded 5×10^3 cells/well (96-well plate) or 2.5×10^5 cells/well (6-well plate).

Sodium Iodate ($NaIO_3$) Induced Damage

Sodium iodate ($NaIO_3$) (Sigma-Aldrich, 71702) is a potent oxidizing agent that selectively targets retinal pigment epithelial (RPE) cells (ED_{50} curve in Supplementary Figure 1). Its application, both in vitro and in vivo, has become a widely recognized and reproducible model for studying age-related macular degeneration (AMD). ARPE-19 cells were seeded in a complete medium and allowed to settle for 24 hours. Next day, the medium was exchanged for DMEM/F12 supplemented with 1% FBS containing 10 mM $NaIO_3$ to induce oxidative stress. Stock solutions of $NaIO_3$ [400 mM] were each time prepared freshly before use by dissolving 50 mg of $NaIO_3$ in 650 µL DMEM/F12. Cells were incubated with $NaIO_3$ for 24 hours. Then, medium was exchanged for complete medium and nanoparticles were added.

Sh-Sy5y

The SH-SY5Y neuroblastoma cell line (human, ECACC; Sigma Aldrich, St. Louis, MO, USA) was cultured in a proliferation medium, consisting of a 1:1 mixture of Ham's F-12 Nutrient Mixture (Thermo Fisher, Waltham, MA, USA) and Minimum Essential Medium (MEM) (Sigma Aldrich, St. Louis, MO, USA), supplemented with streptomycin (100 U/mL), penicillin (100 µg/mL), L-glutamine (2 mM), and 10% heat-inactivated fetal bovine serum (FBS).

Generation of RA-Differentiated SH-SY5Y Cells

SH-SY5Y cells can differentiate into neuron-like cells under specific conditions.[32] Differentiation of SH-SY5Y cells results in extensive neurite outgrowth and the expression of mature neuronal markers (eg, NeuN, β-III tubulin), with the resulting cells adopting either a dopaminergic or cholinergic phenotype that show selective vulnerability in Parkinson's and Alzheimer's diseases.[33] 1.0×10^4 cells/well (96-well plate, Nunclon, Thermo Fisher Scientific, Waltham, MA, USA) or 0.3×10^6 cells/well (6-well plate, Nunclon, Thermo Fisher Scientific, Waltham, MA, USA) were seeded in a reduced serum medium consisting of Minimum Essential Medium, 2mM L-Glutamine and 1% (*v/v*) FBS. Next day medium was supplemented with 10 µM retinoic acid (all trans-retinoic acid, R2625, Sigma). The differentiation medium was exchanged every 2–3 days for 7 days.

6-Hydroxydopamine (6-OHDA) Damage

After differentiation, SH-SY5Y cells were exposed to 25 µM 6-hydroxydopamine (6-OHDA, Sigma) for 24 hours (ED_{50} curve in Supplementary Figure 1). 6-OHDA is a neurotoxin commonly used in in vitro models of neurodegeneration. It selectively targets dopaminergic neurons, leading to their loss, a hallmark of Parkinson's disease. By inducing oxidative stress, mitochondrial dysfunction, and apoptosis, 6-OHDA mimics key mechanisms observed in Parkinson's, including dopamine depletion, neuroinflammation, and neuronal death.[33]

Application of Nanoparticles to Cell Cultures

After 24 hours of initial incubation, oxidative stress was induced with 10 mM $NaIO_3$ or 25 μM 6-OHDA in ARPE-19 or RA-differentiated SH-SY5Y, respectively. The cells were returned to the incubator for 24 hours. Following this, the stress-inducing medium was replaced with DMEM/F12 supplemented with FBS to a final concentration of 10% (*v/v*). Nanoparticle suspensions: HSA-10 μg/mL NT3 - 10 μg/mL BDNF - PEG (NeO10), HSA - 5 μg/mL NT3 - 5 μg/mL BDNF - PEG (NeO5), or PBS buffer (stress control) - were added to the appropriate wells in a 1:9 ratio ($v_{nanoparticle}$:v_{medium}). A suspension of PEGylated HSA (HSA-PEG) nanoparticles was used as an additional control.

Protein Isolation and Relative Quantification

ARPE19 or SH-SY5Y cells were cultured on a six-well plate as described in the previous sections. After 72 hours, cells were trypsynized and centrifuged for 300 x *g* for 5 minutes. Pelleted cells were resuspended in the cell lysing mixture of 1 × RIPA Lysis and Extraction Buffer, 1 × Halt™ Protease Inhibitor Cocktail and 1 × Halt™ Phosphatase Inhibitor Cocktail (Cat. No. 89901, 87786 and 78420 respectively, Thermo Fisher Scientific, Waltham, MA, USA). After 20 min. of incubation at 4 °C, the remains of the cells were centrifuged at 15,000 × *g* in 4 °C for 15 min. Lysates were immediately transferred to −80 °C for future analysis. The quantification of protein concentration in each sample was performed using the BCA protein assay kit for low concentrations (ab207002, Abcam, Cambridge, UK) according to the manufacturer's instruction.

Enzyme-Linked Immunosorbent Assay (ELISA)

To assess cellular uptake, 1 μg of total cell lysate was used for the quantification of HSA (ab108787, Abcam, Cambridge, UK), BDNF (DY248, Bio-techne, MN, USA), and NT3 (DY267, Bio-techne, MN, USA) concentrations. For the vitreous body and retina samples from rabbit eyes, NT3 and BDNF levels were determined. All procedures were performed following the manufacturer's guidelines. In rabbit ocular samples, ELISA quantified extractable neurotrophin levels in vitreous and retinal tissue extracts and did not distinguish intracellular, surface-bound, extracellular matrix-associated, or formulation-associated protein fractions. The levels of proteins were analyzed using GraphPad Prism ver. 9.5.1 software (GraphPad Software, San Diego, California, USA; https://www.graphpad.com).

Cytotoxicity

Jc-1

At low concentrations, JC-1 dye (JC-1 Mitochondrial Membrane Potential Assay Kit, ref. 10009172, Cayman Chemical, MI, USA) occurs as a monomer and is characterized by green fluorescence. In mitochondria, JC-1 can accumulate, creating J-aggregates that emit red fluorescence. The accumulation of JC-1 depends on the mitochondrial membrane potential ($\Delta\Psi_M$). Apoptotic cells are characterized by a low $\Delta\Psi_M$, which is detected as a decrease in red (J-aggregates) to green (J-monomers) fluorescence. Briefly, 5×10^3 ARPE-19 or differentiated SH-SY5Y cells were cultured in 96-well black clear-bottom plates and exposed to oxidative stress as described above. Subsequently, the medium was exchanged for DMEM/F12 10% FBS, and cells were treated with HSA-PEG NPs, NeO5, NeO10 or PBS (untreated stressed control). The nanoparticles were added to the appropriate wells in cell culture medium at a 1:9 ratio ($v_{nanoparticles}/v_{medium}$). After 72 hours of incubation, the cells were stained for 20 minutes with JC-1 dye according to the manufacturer's instructions. Fluorescence was detected with a Varioskan LUX Plate Reader (Thermo Fisher); red fluorescence was read at an excitation wavelength of 535 nm and an emission wavelength of 595 nm, and green fluorescence was read at an excitation wavelength of 485 nm and an emission wavelength of 535 nm. The red (J-aggregates) to green (J-monomers) fluorescence ratio was analyzed with GraphPad prism software.

Annexin V/Propidium Iodide

Annexin V binds with high affinity to phosphatidylserine, a phospholipid that is typically located on the inner leaflet of the cell membrane. Conjugating Fluorescein Isothiocyanate (FITC) to Annexin V allows for the detection of membrane asymmetry, a hallmark of cells undergoing apoptosis. The addition of Propidium Iodide (PI) enables differentiation between early or late apoptotic cells and dead or necrotic cells, as PI enters cells that have compromised membrane integrity and emits red fluorescence (detected in the phycoerythrin (PE) channel). ARPE-19 cells were seeded in 24-well

plate. After 24 hours of pre-incubation, cells were exposed to the oxidative stress as described above. The following day, medium was exchanged for DMEM/F12, and either PBS, PEGylated HSA (HSA-PEG), or NeO10 was added. Cells were incubated for another 48–72 hours. After the indicated time, the cells were trypsinized and washed twice with PBS w/o Mg and Ca and suspended in annexin V staining buffer (556570, BD Biosciences, San Jose, CA, USA). Annexin V-FITC and propidium iodide were added according to manufacturer's instruction. Cells were stained for 15 minutes, and then immediately acquired with a flow cytometer. FCS files were visualized and analyzed with floreada.io (https://floreada.io). Statistical analysis of the percentage of apoptotic and alive cells was performed with GraphPad prism software.

RNA Isolation and RealTime qPCR

Cells were seeded in a 6-well plate. RA-differentiated SH-SY5Y or ARPE-19 cells were exposed to oxidative stress as described above. The following day, cell culture medium was exchanged for DMEM/F12 containing 10% FBS and supplemented with PBS, PEGylated HSA, or NeO10 nanoparticles. After 48 hours, cells were trypsinized and pelleted by centrifugation (5 minutes at 300 x *g*). RNA was isolated with NucleoSpin TriPrep kit (740966, MACHEREY-NAGEL, Düren, Germany). Reverse transcription was performed on 0.5 µg of total RNA (K1622, RevertAid First Strand cDNA Synthesis Kit, Thermo Fisher Scientific). The resulting mixture containing cDNA was diluted 10 times.

The RT qPCR reaction was set with 10 ng of cDNA and 200 nM of each primer. RT-qPCR was performed using the following thermal cycling conditions: initial denaturation at 95°C for 5 min, followed by 39 cycles of denaturation at 96°C for 15s, annealing at 60°C for 30s, and extension at 72°C for 15s, using Bio-rad CFX Maestro software ver. 4.1.2433.1219. Fluorescence signal acquisition was conducted during the annealing step. Primer sequences for rabbit genes are presented in Supplementary Table 1 and for human genes in Supplementary Table 2.

Data from the rabbit's eye was log2-transformed prior to visualization to stabilize variance. Given the limited sample size, no formal inferential statistics were performed. The analysis is therefore descriptive and focuses on the magnitude and direction of observed transcriptional changes across groups. The RT-qPCR panel was designed to assess transcriptional markers associated with MAPK/p38 signaling, the AKT/mTOR axis, and regulators of proliferation and apoptosis. Primers were selected based on available *Oryctolagus cuniculus* sequences (Supplementary Table 1).

Relative gene expression was calculated using the ΔΔCt method with species-specific GAPDH as the endogenous reference gene. Human GAPDH was used for ARPE-19 and SH-SY5Y samples, whereas rabbit Gapdh was used for rabbit ocular tissue samples. Primer sequences are provided in Supplementary Tables 1 and 2.

Detection of Lipid Peroxidation

Lipid peroxidation primarily occurs due to free radical attacks on specific molecules, particularly polyunsaturated fatty acids, leading to oxidative stress. The concentration of malondialdehyde (MDA) in cell cultures serves as a key biomarker for evaluating the extent of this process. After adhering to a 6-well plate, 2.5×10^5 cells per well were incubated with 10 mM $NaIO_3$ (as described in section 2.4.1) for 24 hours. The experimental details were outlined in previous sections. Following the incubation period, the cell supernatant was collected from each well. The MDA concentration in the supernatant was measured using reverse-phase high-performance liquid chromatography (HPLC) combined with a spectrophotometric detection method. This method was performed using an Agilent 1260 Infinity II HPLC system (Agilent Technologies, Waldbronn, Germany)[34] with a BDS Hypersil C18 column. A freshly prepared 10 mM TEP (1,1,3,3-tetraethoxypropane) stock solution was diluted in water to generate working calibrants at concentrations of 0.05, 0.075, 0.1, 0.15, and 0.2 µM TEP. For deproteinization and antioxidant protection, 100 µL of the supernatant or standard was mixed with 200 µL of 5% TCA (trichloroacetic acid) and 10 µL of 0.4% BHT (butylated hydroxytoluene) in absolute ethanol. The samples were then vortexed thoroughly. Next, 100 µL of 0.6% TBA (2-thiobarbituric acid) was added, and the mixture was incubated at 90°C for 45 minutes, allowing the formation of the MDA-$(TBA)_2$ adduct, which was detected at 532 nm. Following centrifugation at 8000 × g for 10 minutes at 4°C, the supernatants were collected and adjusted to pH 7.0 using 1 M NaOH. The elution buffer was composed of 50 mM KH_2PO_4 (adjusted to pH 7.0 with KOH) and methanol (CH_3OH) in a 70:30 (*v/v*) ratio. The total run time for each sample was 6.5 minutes, with a flow rate of 0.5 mL/min, an injection volume of 20 µL, and excitation and emission wavelengths of 528 nm and 553 nm, respectively.[19] The MDA release from human ARPE-19 cells was quantified by integrating

retention times and peak areas, which were then compared to known MDA concentrations. The MDA levels were calculated in mM MDA equivalents based on the TEP standard calibration curve (Supplementary Figure 2), assuming a 1:1 conversion under acidic conditions.

Animal Experiments

Ethical Approval Statement

All animal experiments were approved by the Local Ethics Committee for Animal Experiments in Lublin (University of Life Sciences in Lublin, Akademicka 13, 20–950 Lublin, Poland). The study was conducted under approval no. 75/2022 (issued on 06 June 2022), with a subsequent amendment approved under no. 92/2022 (issued on 19 September 2022).

No separate animal experimentation license number was assigned under applicable national regulations. All procedures were performed in accordance with the ARRIVE 2.0 guidelines, Directive 2010/63/EU of the European Parliament and of the Council on the protection of animals used for scientific purposes, and the Polish Act of 15 January 2015 on the Protection of Animals Used for Scientific or Educational Purposes.

Justification for the Use of Animals

The use of rabbits (*Oryctolagus cuniculus*; n=22; Charles River Laboratories, MA, USA) was essential to evaluate the in vivo biodistribution and stability of the tested nanoparticles. The rabbit eye represents a well-established and relevant model for the human eye due to its similar anatomical and physiological features. Therefore, it was critical for assessing ocular drug delivery and distribution in a biologically meaningful context.

Animal Housing and Welfare Conditions

Prior to the experiment, 12-week-old males underwent a 14-day acclimatization with health monitoring to exclude infections or underlying conditions. Animals were housed individually or in pairs in AK 4200-type cages, depending on their body weight and social compatibility. Each cage was appropriately labeled with an identification card. The room temperature was maintained at 22 ± 2°C with a relative humidity of 50 ± 10%, controlled by an automated ventilation and air-conditioning system. The facility operated on a 12-hour light/dark cycle with artificial lighting.

Throughout the experiment, animals had ad libitum access to fresh water, and a standardized commercial pelleted diet formulated for fur-bearing animals. Environmental enrichment was provided, including wooden blocks for gnawing, aspen tunnels, and nesting materials. Cages were cleaned regularly to maintain hygiene, and air quality was ensured through continuous ventilation.

Animals were provided with a quiet, stress-reduced resting environment. To minimize stress, all handling and experimental procedures were performed by trained personnel following refined protocols. The animals' well-being was assessed daily, and any signs of discomfort or distress were addressed according to ethical guidelines. All procedures were designed to minimize animal suffering and were performed by trained personnel in accordance with approved protocols. The study was reported in accordance with the ARRIVE 2.0 guidelines (https://arriveguidelines.org/).

Experiment

Rabbits received intravitreal injections of 50 µL of (i) NeO10, (ii) NeO100, (iii) PEGylated human serum albumin or (iv) PBS. All procedures were performed under general anaesthesia induced by intramuscular administration of 0.25 mg/kg body weight of medetomidine (Domitor; Orion Pharma, Warszawa, Poland) and 15 mg/kg body weight of ketamine (Ketamina; Biowet Puławy, Puławy, Poland). After the procedure, the rabbit received an antibiotic in the form of an ointment (tobramycin 3 mg/g body weight). The animal's condition was monitored on a heating pad until full recovery from anesthesia, and subsequently in its housing cages. Randomly selected animals were euthanized at predefined time points (72 hours, 28 days). Euthanasia was performed by concussion (mechanical stunning), carried out by a trained and qualified person. This method was used to preserve tissue integrity for immunohistochemical analysis of the eyeballs, which excluded the use of pharmacological agents. All procedures were performed in accordance with approved veterinary standards for laboratory animal care.

Statistics

Statistical analysis was performed with GraphPad Prism ver. 10.6 software for Windows (GraphPad Software, San Diego, California, USA; https://www.graphpad.com).

Results

Physicochemical Characterization and Stability of PEGylated HSA-NT3-BDNF Nanoparticles

Although the PEGylated albumin platform was previously described[16] using a single neurotrophin loading (10 mg/L), the present study includes two formulations differing in cargo concentration (5 mg/L and 10 mg/L; NeO5 and NeO10). This design enables assessment of formulation robustness across loading conditions while providing a well-characterized basis for subsequent translational evaluation in cellular stress models and in vivo studies.

Variations in cargo concentration may alter intermolecular interactions within the albumin matrix and thereby affect nanoparticle size, dispersity, and surface charge. As protein loading density can modulate surface adsorption, hydration shell organization, and PEG–protein packing, comprehensive physicochemical re-characterization was required prior to biological evaluation to confirm consistent platform performance.

MADLS analysis revealed reproducible size distributions for both formulations (Figure 2A and B). The hydrodynamic diameters ranged from 5.9 ± 1 nm to 54.2 ± 3 nm, indicating well-defined nanoparticle populations rather than aggregation. Representative MADLS distributions of scattering intensity and number, together with autocorrelation functions for the NeO5 formulation, are additionally presented in Supplementary Figure 3, demonstrating stable nanoparticle populations over the entire 28-day storage period with minimal changes in peak position and distribution profile.

Notably, variations between NeO5 and NeO10 suggest that neurotrophin loading concentration influences nanoscale organization of the PEGylated albumin matrix. Such concentration-dependent effects are expected, as increased protein

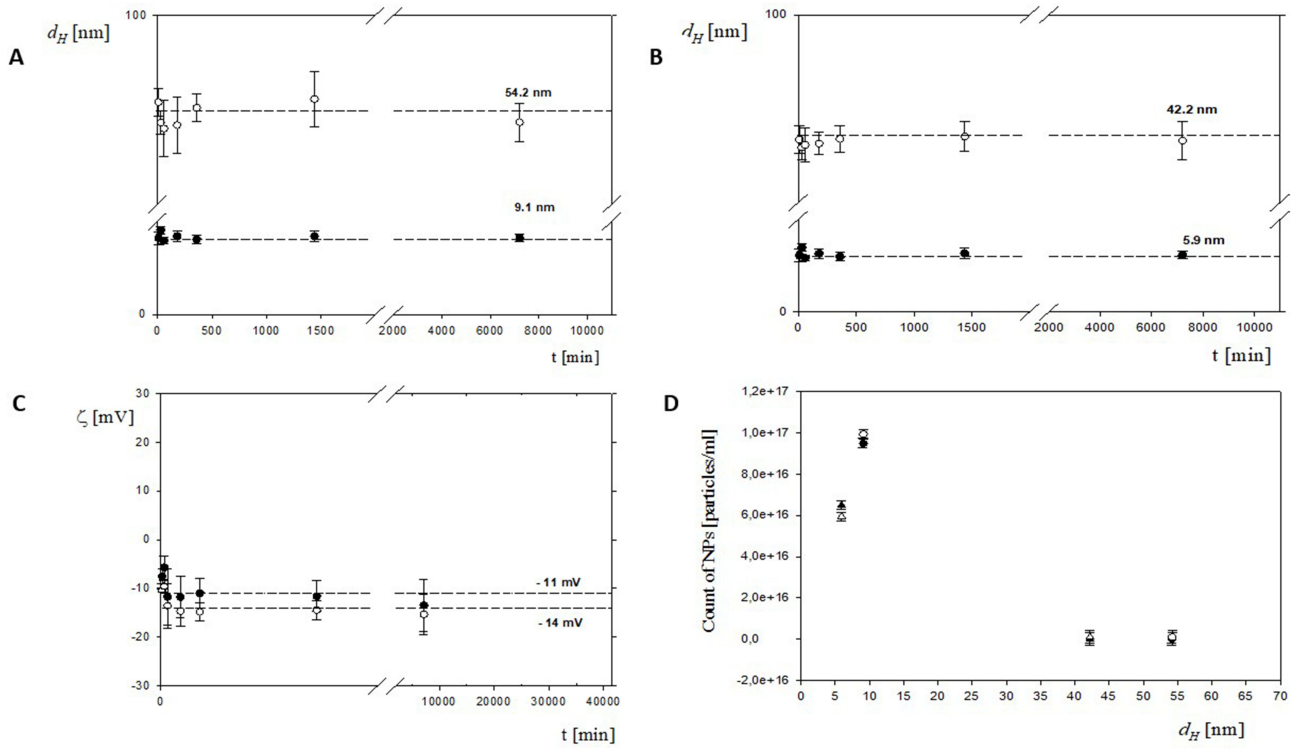

Figure 2 Physicochemical characterization of PEGylated HSA-NT3-BDNF nanoparticles over 28 days (40,320 min) after formulation. Particle size distributions were measured by intensity (**A**) NeO 10; (**B**) NeO 5. (**C**) ζ -potential was measured in Ringer's solution (open symbols: NeO 5; filled symbols: NeO 10). Particle concentrations for NeO 10 and NeO 5 were determined by MADLS (**D**). All syntheses were performed in six replicates, and error bars denote mean ± SD. Individual points represent NP diameter distributions obtained from eight samples.

https://doi.org/10.2147/IJN.S608949

content may modify surface packing density and internal structural arrangement. The polydispersity indices (PDI = 0.18 ± 0.02) remained below 0.3 for both formulations, indicating narrow size distributions and colloidal homogeneity. Maintaining low dispersity is critical, as heterogeneous nanoparticle populations may exhibit variable cellular uptake kinetics, inconsistent cargo release, and unpredictable biological responses. The consistently low PDI confirms controlled assembly despite differences in protein loading. ζ -potential measurements performed in Ringer's solution showed moderately negative surface charge values (−11 ± 1.2 mV for NeO5 and −14 ± 0.7 mV for NeO10; Figure 2C). The slight differences between formulations further support the influence of cargo concentration on surface electrostatics. At physiological ionic strength, PEGylated systems rely primarily on steric stabilization; therefore, a stable hydrodynamic diameter and moderate ζ -potential values confirm colloidal stability without aggregation. MADLS-based particle concentration analysis (Figure 2D) demonstrated reproducible nanoparticle counts across independent batches (n = 3), confirming the consistency of synthesis across protein-loading conditions. Collectively, these data demonstrate that altering neurotrophin concentration within PEGylated HSA nanoparticles modulates physicochemical parameters while preserving nanoscale stability and colloidal integrity over 28 days (Figure 2A–C).

A qualitative analysis of the AFM micrographs confirmed that PEGylated HSA/BDNF/NT3 nanoparticles maintain a consistent spherical shape with minimal size variation. Importantly, no elongated aggregates or filamentous structures were detected throughout the 28-days (Figure 3). These results confirm that the PEGylated HSA platform maintains physicochemical stability over time, supporting its suitability for biological experiments.

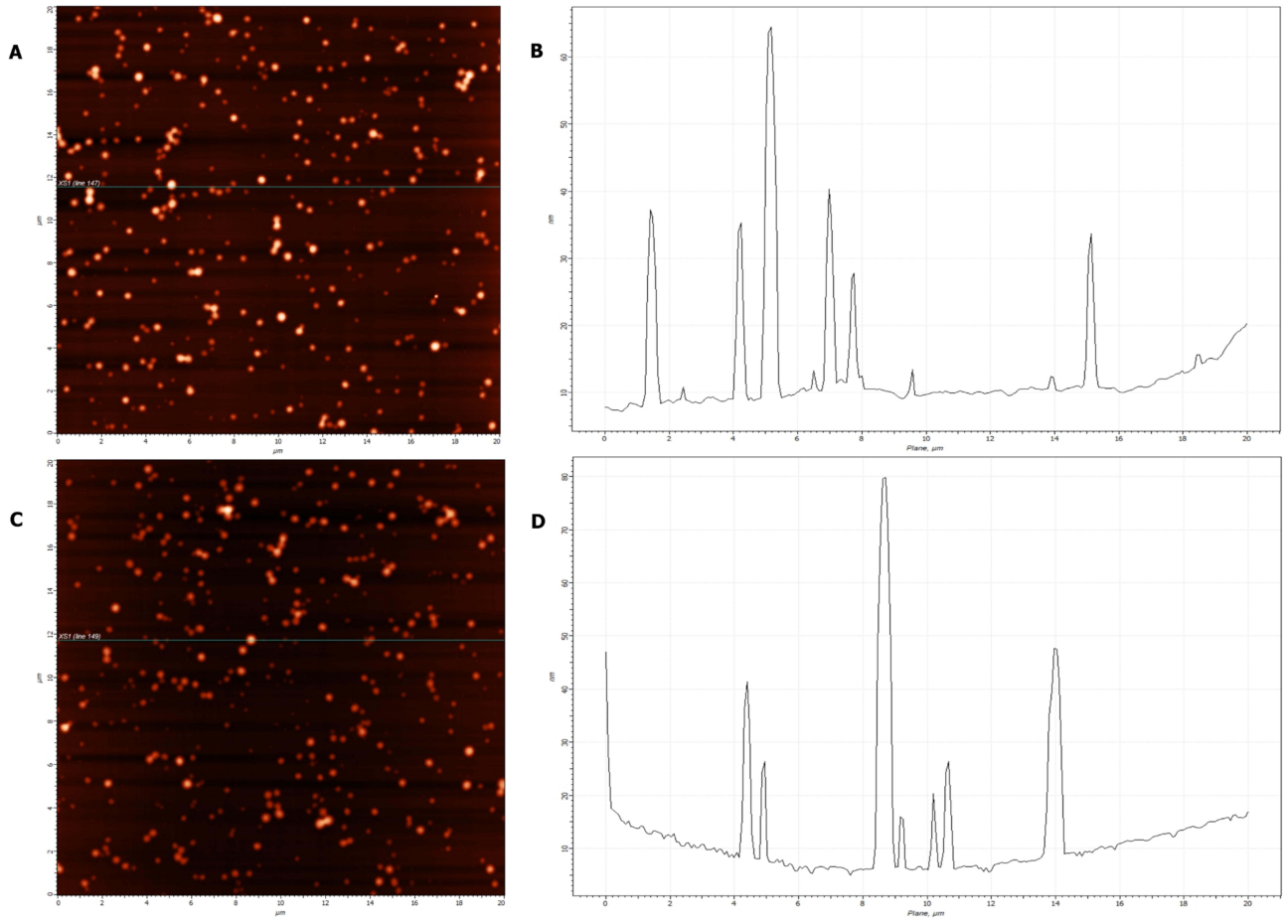

Figure 3 AFM characterization of PEGylated HSA-NT3-BDNF nanoparticle diameter distribution over 28 days after formulation. AFM images of nanoparticles deposited from Ringer's solution at pH 7.0 ± 0.6 are shown 24 h (**A**) and 28 days (**C**) after formulation, with corresponding X-axis cross-sections (**B** and **D**) acquired over a 20×20 µm area. Notably, the dispersed morphology of PEGylated NT3-BDNF nanoparticles was preserved over 28 days (40,320 min).

Intraocular Distribution and Safety-Related Readouts in the Rabbit Eye

To assess platform performance in a second species, PEGylated HSA nanoparticles were administered intravitreally into the rabbit eye. No macroscopic signs of ocular irritation, edema, or hemorrhage were observed during the observation period following injection.

In our previous work, we demonstrated that PEGylated human serum albumin-based nanoparticles enable controlled co-delivery of BDNF and NT3, significantly prolonging the half-life of these neurotrophins.[16] Here we sought to evaluate neurotrophins persistence and early tissue-level molecular responses following intravitreal administration in the rabbit eye, representing a distinct ocular environment and a second species (Figure 4A and B).

ELISA-based protein quantification showed detectable BDNF levels in both the vitreous body and retinal tissue extracts 72 h after administration. After 28 days, BDNF was no longer detectable, indicating a transient persistence within rabbit ocular tissues under the tested conditions. In contrast, NT3 was not detectable in vitreous or retinal tissue extracts at either time point. These findings indicate differential persistence of the two neurotrophins in the rabbit eye and highlight species- and cargo-dependent aspects of platform performance.

To characterize transcriptional responses at early (72 h) and later (28 days) time points in rabbit ocular tissues, we selected a panel of rabbit transcripts associated with key pro-survival, proliferation-, and apoptosis-related signaling pathways, including MAPK/p38 signaling (*Cnksr2, Mknk1, Mapkapk2, Mapkapk3*), the AKT/mTOR axis (*Akt1, Mtor*), the CREB-associated co-activator (*Crebbp*), the NFκB-associated regulator (*Nkap*), and regulators of proliferation and apoptosis (*Pcna, Bcl2, Casp3, Tp53*) (Figure 4C). Due to the limited number of biological replicates, the results are presented descriptively to illustrate directional trends rather than to support statistical inference. Individual sample-level expression values are provided in Supplementary Figure 4 to illustrate inter-sample variability. Gene expression patterns are visualized as standardized heatmaps to facilitate comparison across treatment groups and time points.

At 72 h, transcriptional modulation across all experimental groups was generally modest and heterogeneous. Notably, relative deviations from intact levels appeared more pronounced in the Ringer-treated group for several transcripts, whereas nanoparticle-treated groups (NeO10 and NeO100) tended to remain closer to baseline expression. Given the exploratory nature of the analysis, this pattern may suggest that early transcriptional changes primarily reflected responses to vehicle administration or injection-related tissue perturbation rather than nanoparticle-specific effects. At 28 days, the Ringer-treated group remained largely comparable to intact controls, whereas nanoparticle-treated groups exhibited more pronounced transcriptional deviations. In particular, *Pcna* and *Mapkapk3* expression levels were relatively higher in NeO-treated tissues. Moderate increases in *Tp53* and *Bcl2* were also observed, while *Casp3* expression did not demonstrate a coordinated increase across groups.

Functional Delivery Under Oxidative Stress Conditions

To evaluate whether neurotrophins delivered via PEGylated HSA nanoparticles retain biological functionality under adverse conditions, oxidative stress was selected as a biologically relevant and broadly applicable challenge, as it represents a common cellular stressor known to compromise protein stability and cell viability. Since both NT3 and BDNF are human proteins, interspecies differences may influence their stability, persistence, or downstream molecular responses following administration in rabbit ocular tissues. To complement the in vivo findings and to assess cargo functionality in a homologous cellular context, nanoparticle-mediated delivery of neurotrophins was therefore evaluated in human epithelial and neuronal cell models under oxidative stress conditions.

Oxidative stress was induced using 6-OHDA in RA-differentiated SH-SY5Y cells (Figure 5A) and $NaIO_3$ in ARPE-19 cells (Figure 5B). Mitochondrial integrity was assessed using the JC-1 assay, and the data are expressed as the ratio ± standard deviation of J-aggregates to J-monomers (raw fluorescence intensities in Supplementary Figure 5), a widely used readout of mitochondrial membrane potential. Exposure to $NaIO_3$ reduced ARPE-19 cell viability to 10.0 ± 1.74 compared with 19.2 ± 0.8 in the untreated control, whereas 6-OHDA decreased viability of SH-SY5Y cells to 2.1 ± 0.1 vs 5.3 ± 0.3 in untreated control, confirming effective induction of oxidative stress in both systems. There was no difference between 6-OHDA treated group and group treated with 6-OHDA and then solely addition of free NT3 and/or BDNF on viability and mitochondrial membrane potential in 6-OHDA-stressed RA-differentiated SH-SY5Y cells (Supplementary Figure 6).

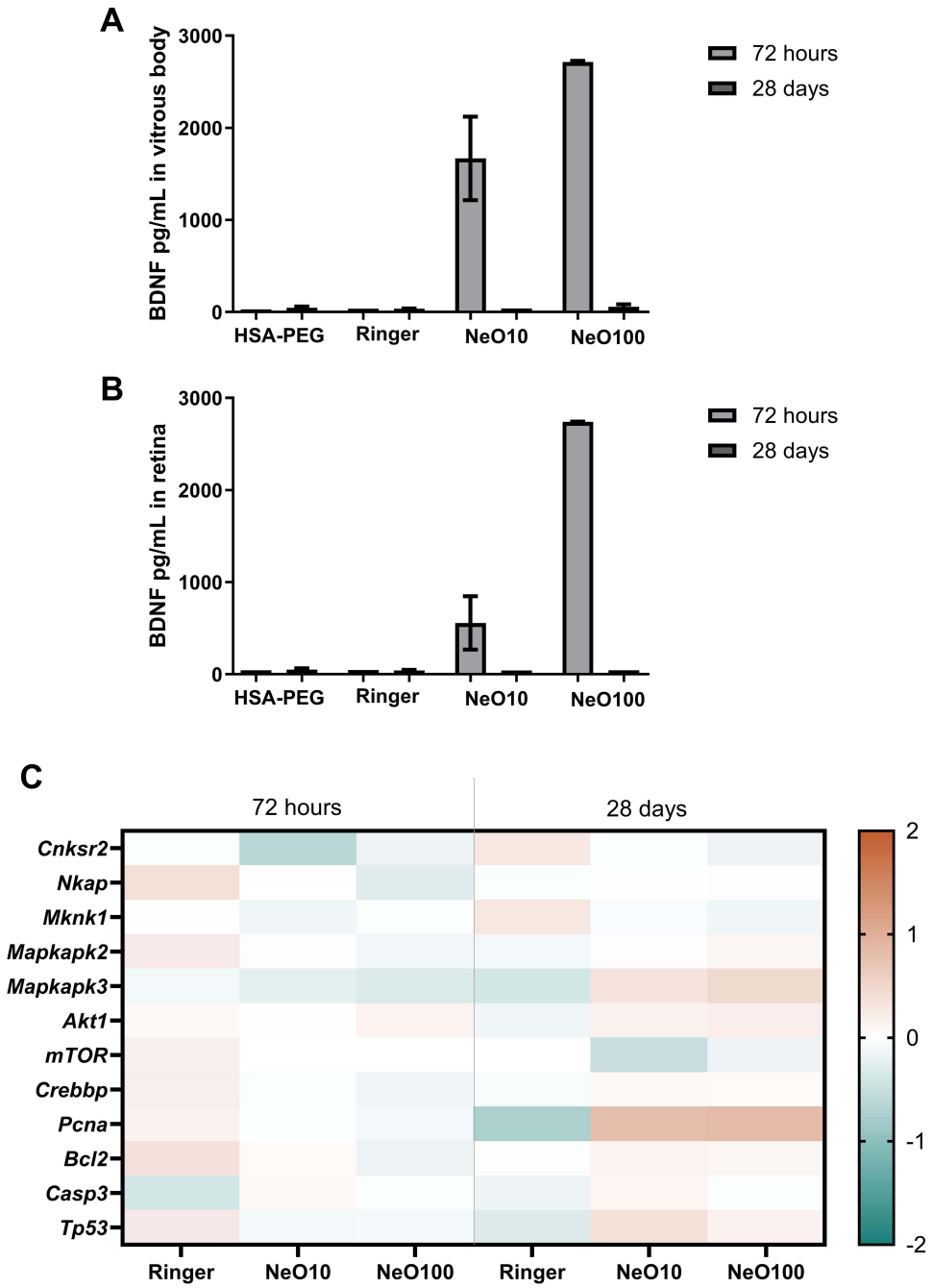

Figure 4 BDNF levels and associated transcriptional profiles in rabbit ocular tissues at 72 hours and 28 days following nanoparticle administration. (**A**) BDNF concentrations in the vitreous body and (**B**) retina of rabbits' eyes measured at 72 hours and 28 days after administration of vehicle (Ringer), HSA-PEG NPs, or nanoparticle formulations (NeO10, NeO100). Data are presented as mean ± SD (n = 3 biological replicates per group). (**C**) Heatmap representation of relative mRNA expression levels of selected rabbit genes associated with MAPK/p38 signaling (*Cnksr2, Nkap, Mknk1, Mapkapk2, Mapkapk3*), AKT/mTOR axis (*Akt1, Mtor*) CREB- *(Crebbp*) and NFκB-related (*Mknk1*) transcriptional regulation, and proliferation/apoptosis (*Pcna, Bcl2, Casp3, and Tp53*). Gene expression was quantified by RT-qPCR using the $2^{-\Delta\Delta Ct}$ method, with intact control samples serving as calibrator (set to 1). Values were log2-transformed prior to visualization to allow symmetric representation of relative up- and downregulation (log2 fold change relative to control). Samples were analyzed at early (72 h) and late (28 days) time points following treatment with Ringer, NeO10, or NeO100. The color scale indicates relative expression changes compared with intact control, with red tones representing higher relative expression and blue tones representing lower relative expression. Each column represents the mean expression value per group (n = 3 biological replicates). Given the limited sample size, no formal inferential statistical testing was performed; the analysis is presented as exploratory and descriptive, focusing on directional trends and relative magnitude of change rather than statistical significance. Individual sample-level expression values are provided in Supplementary Figure 1 to illustrate inter-sample variability.

Treatment with PEGylated HSA nanoparticles carrying BDNF and NT3 resulted in consistently higher cell viability under identical stress conditions. In ARPE-19 viability increased to 19.2 ± 0.72 and 17.44 ± 0.4, after exposure to HSA-PEG or Neo10, respectively. Similarly, in RA-differentiated SH-SY5Y cells, viability was restored to 3.2 ± 0.1 and 3.5 ± 0.1.

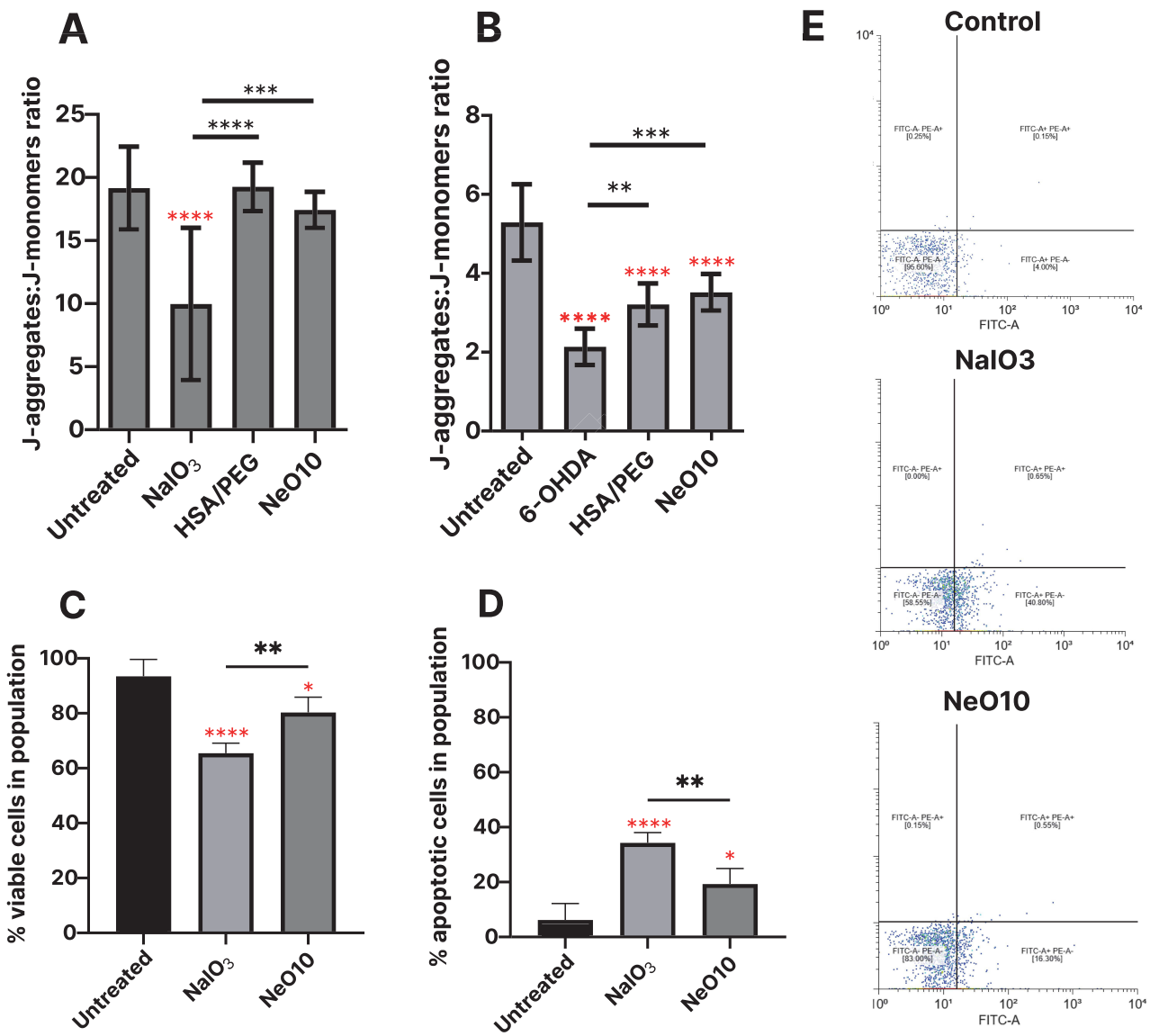

Figure 5 Apoptosis assessment by flow cytometry (Annexin V/PI staining) and JC-1 assay. JC-1 reveals mitochondrial depolarization expressed as the J-aggregates to J-monomer fluorescence ratio in SH-SY5Y (**A**) and ARPE-19 (**B**) cells following treatment with 6-OHDA and $NaIO_3$, respectively. Quantification of viable (Annexin V-negative, (**C**) and early apoptotic (Annexin V-positive, (**D**) cells. (**E**) shows representative flow cytometry dot plots distinguishing viable, early apoptotic, and late apoptotic/necrotic populations. Data presented as mean±SEM from biological triplicate. Data was analyzed using one-way ANOVA with Tukey's multiple comparisons test (GraphPad software) *p>0.05, **p<0.01, ***p< 0.001, ****p< 0.0001. Red stars are statistical significance in relation to control.

To further characterize stress-induced changes in cell fate, mitochondrial membrane integrity and cell viability were assessed by flow cytometry using Annexin V and propidium iodide staining, enabling discrimination between viable, apoptotic, and necrotic cell populations (Figure 5C–E). $NaIO_3$ exposure reduced the proportion of viable ARPE-19 cells to 65.4 ± 1.8%, whereas treatment with NeO10 increased the percentage of viable cells to 80.3 ± 2.3%. Correspondingly, the fraction of apoptotic cells was lower in NeO10-treated cultures (19.3 ± 2.3%) compared to $NaIO_3$-stressed controls without further treatment (34.3 ± 1.9%) (Figure 5E).

Oxidative stress levels were additionally quantified by measuring MDA concentration, a well-established marker of lipid peroxidation, in the cell culture supernatants using HPLC (Figure 6). Using this method, we observed that treatment with HSA-PEG, NeO5, and NeO10 nanoparticles significantly reduced MDA levels in ARPE-19 cells compared to both untreated and stressed controls. Notably, MDA was nearly undetectable in samples treated with Neo10, indicating a pronounced

https://doi.org/10.2147/IJN.S608949

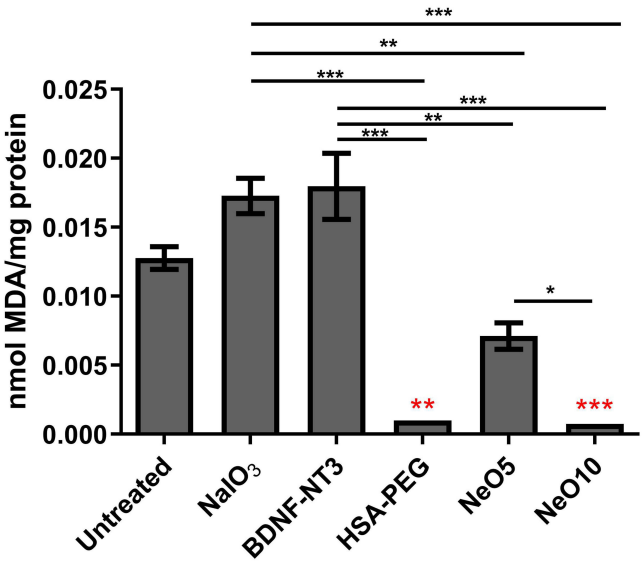

Figure 6 Assessment of MDA concentration in ARPE19 cell supernatant after 48 hours. ARPE19 cells were exposed to 10 mM $NaIO_3$, NeO5, NeO10, HSA-PEG or BDNF/NT3 (10 mg L^{-1}). MDA levels were normalized to the total protein concentration in each supernatant sample. Data presented as mean±SEM from at least three biological replicates. Statistical significance was determined using the one-way ANOVA: ***p < 0.001, **p < 0.01, *p < 0.05. Red stars are significance in relation to control.

attenuation of oxidative stress in the cell culture medium following nanoparticle-mediated delivery of neurotrophins. Representative chromatograms of MDA standards and experimental samples are presented in Supplementary Figure 2.

Importantly, treatment with empty carrier alone did not fully reproduce the observed effects, indicating that the reduction in apoptosis-associated readouts and oxidative stress markers was associated with the presence of neurotrophic cargo rather than the albumin-based carrier itself. Comparable trends were observed across oxidative stress paradigms, supporting preservation of neurotrophin functionality following delivery by PEGylated HSA nanoparticles under conditions of cellular stress.

Cellular Uptake and Intracellular Localization of the Nanoparticle Platform

Intracellular levels of NT3 and BDNF were quantified by ELISA as a direct and quantitative readout of nanoparticle-mediated cargo delivery into human cells. Following oxidative stress induction, ARPE-19 cells were treated with $NaIO_3$, whereas RA-differentiated SH-SY5Y cells were challenged with 6-OHDA.

Treatment with PEGylated HSA nanoparticles carrying neurotrophins resulted in a pronounced increase in intracellular concentrations of both BDNF and NT3 compared to untreated controls (Figure 7). In SH-SY5Y cells, intracellular BDNF levels reached 281.4 ± 15.1 ng/mL, whereas untreated cells contained 7.2 ± 0.5 ng/mL. Similarly, ARPE-19 cells exhibited intracellular BDNF concentrations of 216.0 ± 4.1 ng/mL, compared to 6.2 ± 1.2 ng/mL in untreated controls (Figure 7A).

A comparable pattern was observed for NT3. Intracellular NT3 concentrations increased to 159.5 ± 84.8 ng/mL in SH-SY5Y cells and 248.6 ± 11.3 ng/mL in ARPE-19 cells, whereas untreated controls exhibited only 8.4 ± 0.1 ng/mL and 4.4 ± 0.3 ng/mL, respectively (Figure 7B). These data demonstrate efficient intracellular delivery of both neurotrophins mediated by the PEGylated albumin-based nanoparticle platform.

Intracellular levels of HSA were quantified in parallel as a surrogate marker of nanoparticle carrier internalization. In ARPE-19 cells, intracellular HSA increased following exposure to PEGylated HSA alone (21.5 ± 1.3 ng) and NeO10 (18.7 ± 1.3 ng) (Figure 7C). In SH-SY5Y cells, HSA uptake was modestly higher when albumin was co-delivered with neurotrophins, with intracellular levels of 28.7 ± 15.3 ng for HSA-PEG and 31.3 ± 11.4 ng and 31.4 ± 15.2 ng for NeO5 and NeO10, respectively. These data indicate cell-type–dependent differences in albumin uptake while confirming efficient internalization of the nanoparticle carrier.

In ARPE-19 cells (Supplementary Figure 7), both FCGRT and SPARC expression levels were significantly reduced relative to untreated controls across all treatment conditions. In contrast, RA-differentiated SH-SY5Y cells (Supplementary Figure 8) exhibited a significant increase in SPARC expression following HSA-PEG treatment, while

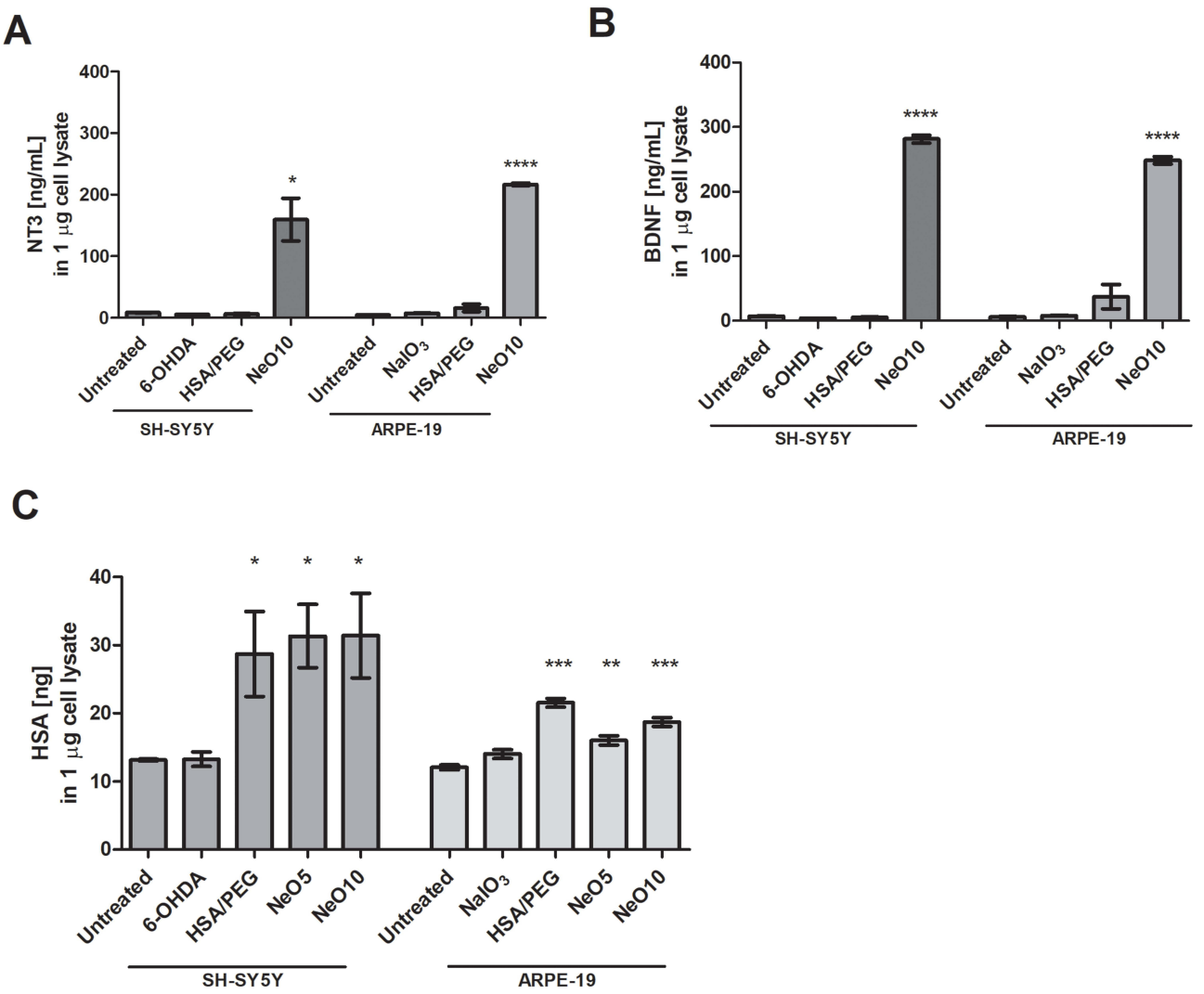

Figure 7 The uptake of BDNF, NT3 and human serum albumin from cell culture medium. SH-SY5Y or ARPE19 cells were exposed to oxidative stress (treated with 6-OHDA or NaIO3, respectively) and subsequently treated with HSA-PEG, Neo5, or Neo10 in cell culture medium. Untreated controls were unstressed. 6-OHDA or NaIO3 controls after stress induction were maintained in regular cell culture medium. Graphs show concentration of intracellular BDNF (**A**), NT3 (**B**) or HSA (**C**) in 1 μg of total cell lysate. Data presented as mean±SEM from biological triplicate at least. Statistical analysis (treated samples versus untreated control) was done in GraphPad Prism using one-way ANOVA with Tukey's multiple comparisons test *p>0.05, **p<0.01, ***p< 0.001, ****p< 0.0001.

no comparable changes were observed for FCGRT. These findings indicate cell-type–dependent regulation of albumin-associated receptors without evidence of coordinated receptor upregulation driving nanoparticle uptake. Consistent with efficient intracellular delivery, qualitative morphological assessment of RA-differentiated SH-SY5Y cells revealed preserved neuronal-like features following exposure to neurotrophin-loaded nanoparticles (Figure 8). These phenotypic observations provided a rationale for subsequent analysis of neurotrophin-related signaling and transcriptional responses.

Neurotrophin-Related Transcript Responses

To provide supportive molecular context for the observed cellular responses, expression of selected neurotrophin-associated signaling markers was assessed. mRNA levels of *TRKB, TRKC, p75NTR*, and the downstream transcription factor *CREB* were quantified by RT-qPCR (Figures 1 and 9). As a reference, the responses to the free protein control is shown on Supplementary Figure 9.

Treatment with NeO10 was associated with increased *TRKB* mRNA expression in both SH-SY5Y (7.8 ± 2.8) and ARPE-19 (2.6 ± 0.4) cells (Figure 9A). A corresponding increase in *CREB* expression was also observed (1.7 ± 0.3 and 2.5 ± 0.6, respectively; Figure 9D). In contrast, *TRKC* expression exhibited only minor, non-significant changes in both

https://doi.org/10.2147/IJN.S608949

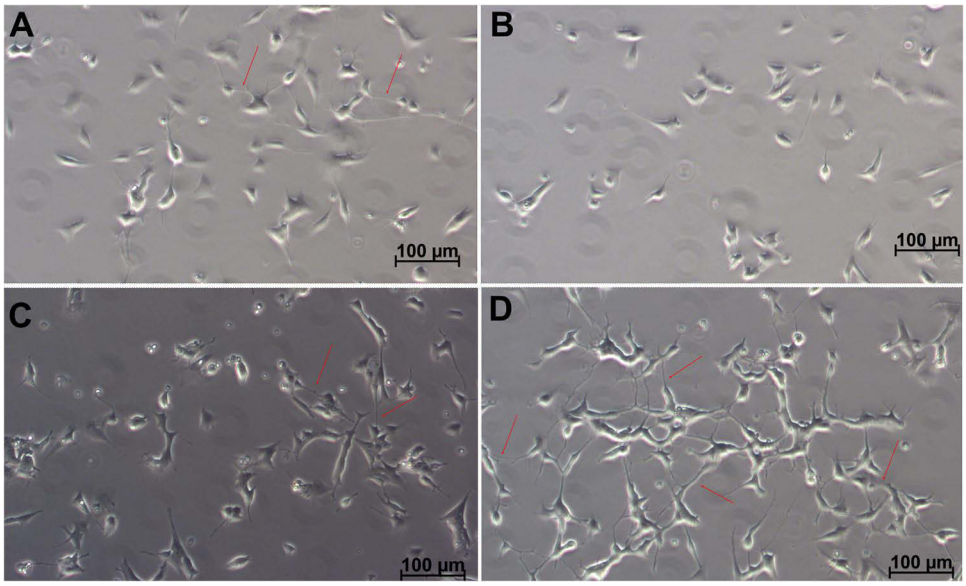

Figure 8 Morphological changes in SH-SY5Y cells following neurodifferentiation. Representative images of SH-SY5Y cells differentiated with retinoic acid and subsequently maintained for one week in (**A**) differentiation medium alone or (**B**) supplemented with either HSA-PEG, (**C**) 10 µg/mL of NT3 and BDNF, or (**D**) NeO10. Cells treated with NeO10 exhibit enhanced morphology and increased formation of intercellular connections (arrowheads). Scale bar: 100 µm.

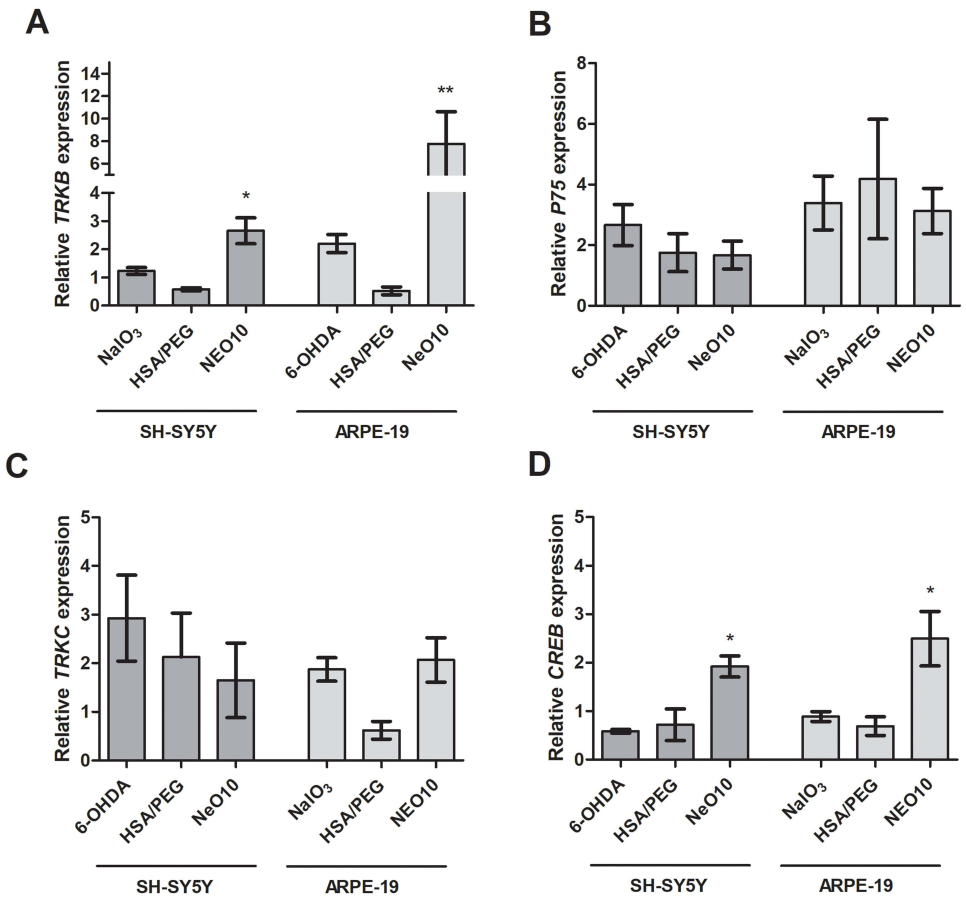

Figure 9 mRNA expression profiles in response to Neo10 treatment following oxidative stress. SH-SY5Y or ARPE19 cells were exposed to oxidative stress (6-OHDA or $NaIO_3$, respectively) or unstressed (untreated). Subsequently, cells were treated with PBS (marked as 6-OHDA or $NaIO_3$) HSA-PEG, Neo5, or Neo10 in regular cell culture medium. Panels show the expression of BDNF/NT3 receptors *TRKB* (**A**), *p75NTR* (**B**), *TRKC* (**C**) and transcription factor *CREB* (**D**). Data presented as mean±SEM from biological triplicate at least. Statistical analysis was done in GraphPad Prism using one-way ANOVA with Tukey's multiple comparisons test *p>0.05, **p<0.01.

cell types, while *p75NTR* expression increased primarily in response to oxidative stress, with the highest levels observed in stressed cells not treated with HSA-PEG or NeO10 (Figure 9B and C, accordingly).

Overall, these transcript-level changes provide supportive molecular context for the functional effects observed after nanoparticle-mediated neurotrophin delivery, but should not be interpreted as direct evidence of protein-level signaling activation.

Discussion

This study extends the evaluation of a PEGylated human serum albumin–based nanoparticle platform designed for the delivery of neurotrophic proteins, with a particular focus on its robustness, biological compatibility, and functional performance across multiple experimental contexts. Building on our previous proof-of-concept work,[16] the present investigation was designed to move beyond single-model validation and instead assess whether the platform maintains predictable behavior when challenged by differences in species, cellular environment, and biological stress. Such cross-context evaluation is increasingly recognized as a critical step in the translational development of protein-based delivery systems.

Although the PEGylated albumin platform was previously introduced,[16] that work examined a single neurotrophin loading condition. In the present study, we deliberately reassessed the system using two cargo concentrations to determine whether altering protein density modifies nanoparticle architecture or compromises colloidal stability. This step is essential because protein loading can influence intermolecular packing, surface electrostatics, hydration shell organization, and PEG chain conformation—parameters that are known to govern nanocarrier stability and biological fate.[19,35] The maintained nanoscale organization following dual neurotrophin incorporation indicates that the albumin matrix tolerates variations in cargo density without structural destabilization. Nanoparticle size is a primary determinant of endocytic uptake pathway selection, intracellular trafficking, and tissue diffusion.[17,36] Importantly, increasing protein loading did not induce aggregation or uncontrolled particle growth, suggesting balanced electrostatic and steric interactions within the PEGylated albumin network rather than disruptive surface overloading. The nanoparticle system was formed via spontaneous self-assembly and steric/electrostatic stabilization within the PEGylated albumin network. Low dispersity across formulations further supports controlled supramolecular assembly. High polydispersity is frequently associated with unpredictable biodistribution, variable release kinetics, and inconsistent cellular uptake.[37] Maintaining monodisperse populations is therefore considered a critical quality attribute in nanomedicine development.[38] Surface electrokinetic behavior provides additional mechanistic insight. While the observed ζ -potential values fall within a moderate range, PEGylated systems rely predominantly on steric stabilization rather than purely electrostatic repulsion.[27,29] The stability of hydrodynamic size and ζ -potential over time supports effective PEG-mediated interparticle spacing and reduced aggregation propensity under physiological ionic strength. Subtle formulation-dependent differences in surface charge further indicate that cargo density modulates interfacial organization without disrupting global electrostatic balance.[39–42] AFM imaging corroborates these findings at the morphological level. The preserved spherical architecture and absence of fibrillar aggregates suggest that PEGylation mitigates protein self-association - a phenomenon commonly observed in free neurotrophin solutions under physiological conditions. Such steric shielding effects of PEG have been extensively documented in protein-based nanocarriers.[16,27,29,39–43]

Evaluation of the platform in the rabbit eye enabled assessment of local exposure and tissue-level responses in a second species without introducing disease-related confounders. In contrast to our previously reported mouse data,[16] where nanoparticle-mediated delivery supported neurotrophin detection for up to 28 days, BDNF was detectable in the rabbit eye at 72 h but not at 28 days, while NT3 was not detected at either time point. The differential detectability of BDNF and NT3 may reflect differences in their interaction with the HSA-based carrier. In our previous work, BDNF showed substantially stronger interaction with HSA than NT3, as indicated by estimated Kd values of 1.6 μM and 732 μM, respectively.[16] This difference may contribute to distinct release and persistence profiles after intravitreal administration. Thus, the absence of detectable NT3 in rabbit ocular tissues may result from faster release, clearance, proteolytic degradation, and/or lower assay detectability, rather than indicating lack of initial incorporation into the formulation. Because no intermediate time points were included, these data indicate transient ocular persistence under the tested conditions rather than a complete clearance profile. Although BDNF and NT3 are evolutionarily conserved across mammals,[44] species-related differences in the ocular microenvironment, including vitreous volume, fluid turnover, local immune environment, proteolytic activity, and protein clearance mechanisms, may influence nanoparticle persistence and

neurotrophin detectability. Therefore, the rabbit findings should be interpreted as a cross-species validation step rather than a direct predictor of human intraocular persistence. These factors should be considered in future studies, particularly when selecting dose levels, sampling intervals, and methods for safety assessment.

Importantly, beyond absolute protein persistence, we sought to determine whether nanoparticle administration elicited measurable cellular responses within ocular tissues. From a translational perspective, two aspects were central within this exploratory rabbit analysis: whether the selected transcript panel showed a coordinated pro-apoptotic pattern and whether transcriptional trends were compatible with pro-survival or regenerative pathway modulation. Across both analyzed time points, the selected transcript panel did not reveal a consistent pattern suggestive of sustained apoptotic or degenerative activation, including a coordinated upregulation of pro-apoptotic markers following nanoparticle administration. At 28 days, the observed trends within regulatory, proliferation-associated, and stress-response markers, including *Pcna, Mapkapk3, Bcl2*, and *Akt1*, were compatible with low-level tissue adaptation rather than a degenerative or pro-apoptotic transcriptional pattern. However, given the limited sample size and descriptive nature of the rabbit analysis, this interpretation should be considered exploratory. Given the limited sample size and descriptive nature of the rabbit analysis, the observed transcriptional trends should be interpreted cautiously. Overall, these exploratory findings did not reveal a coordinated pro-apoptotic transcriptional response and may be consistent with adaptive tissue-level modulation rather than overt cytotoxic disruption. In addition, the absence of histopathological evaluation limits conclusions regarding ocular safety and should be addressed in future studies together with structural and inflammatory ocular assessments.

Similarly, in human cells exposed to oxidative stress, transcriptional changes in neurotrophin-associated markers were directionally consistent with preserved cargo activity. Importantly, these mRNA-level data are not interpreted as evidence of pathway activation but rather as supportive indicators that nanoparticle-mediated delivery does not elicit disruptive or adverse molecular responses during early exposure. The selected transcriptional markers were chosen based on their established association with BDNF- and NT3-mediated signaling. Observed increases in *TRKB* and *CREB* expression (Figure 9) are directionally consistent with preserved neurotrophin activity, as previously reported for both BDNF and NT3.[34,45–48] The biological response to NeO10 was interpreted based on the convergence of complementary experimental readouts rather than on any single assay. Targeted RT-qPCR provided supportive molecular context, whereas functional assays indicated attenuation of oxidative stress-associated cytotoxicity, including changes in mitochondrial membrane potential, apoptosis-related cell populations, and malondialdehyde levels. MDA was interpreted as an oxidative damage marker reflecting lipid peroxidation.[49] Together, these measurements provide an integrated picture consistent with preserved biological activity of nanoparticle-delivered neurotrophins under the tested stress conditions. This observation aligns with previous reports describing the protective role of neurotrophins, including BDNF and NT3, in counteracting oxidative stress.[4] Interestingly, NeO10 elicited the most pronounced effect, rendering MDA levels nearly undetectable, whereas under the same conditions, the NT3 and BDNF combination displayed a markedly weaker response. Additional free-protein controls provided in the Supplementary Material (Supplementary Figure 6 and Supplementary Figure 9) further support this interpretation. In ARPE-19 cells, free NT3/BDNF exposure induced transcript-level changes in selected neurotrophin-related receptors, particularly TRKC and p75NTR, consistent with known NT3 receptor interactions (Supplementary Figure 9). This pattern should not be interpreted as evidence of a defined functional outcome, but it indicates that free neurotrophin exposure elicits a receptor-related transcript response distinct from that observed after nanoparticle treatment. This distinction is important because exposure to free neurotrophins is not directly equivalent to nanoparticle-mediated delivery, where the cargo remains carrier-associated and may be released over time. Moreover, our previous studies showed that free BDNF at comparable concentrations may exert cytotoxic effects in selected cellular settings, supporting the need for controlled carrier-mediated delivery.[16,50] In RA-differentiated SH-SY5Y cells, free NT3, free BDNF, or combined NT3/BDNF did not prevent the 6-OHDA-induced reduction in mitochondrial membrane potential under the tested conditions (Supplementary Figure 6). In contrast, nanoparticle-mediated delivery was associated with improved functional outcomes after oxidative challenge. Together, these data support the interpretation that simple exposure to free neurotrophins does not fully reproduce the biological profile observed after nanoparticle-mediated delivery.

HSA has long been recognized as an attractive carrier for therapeutic agents; however, the intracellular date of albumin-based nanoparticles following uptake remains incompletely understood.[17] Albumin can undergo cellular recycling or degradation, processes known to involve pathways such as FcRn-mediated trafficking and SPARC-associated internalization.[51–53] In the

present study, increased intracellular levels of HSA were detected in both ARPE-19 and SH-SY5Y cells, confirming effective carrier internalization while revealing cell-type–dependent differences in uptake magnitude. Notably, neurotrophin-loaded PEGylated HSA nanoparticles were associated with higher intracellular HSA accumulation in SH-SY5Y cells compared to PEGylated HSA alone, whereas ARPE-19 cells exhibited more modest changes. This might be related to *TRKB* expression, as neural cells are known to internalize BDNF, a key player in synapse formation and differentiation.[54,55] These observations suggest that cellular context influences albumin nanoparticle handling, potentially reflecting differences in metabolic state or neurotrophin responsiveness, rather than indicating a single dominant uptake mechanism. Because intracellular HSA levels differed between ARPE-19 and SH-SY5Y cells, *SPARC* and *FCGRT*/FcRn transcripts were assessed as well-established albumin-associated markers to provide biological context for carrier handling in these cell types. The observed cell-type-dependent transcript patterns suggest that albumin-associated cellular handling may differ between epithelial and neuronal-like cells and is unlikely to be explained by uniform upregulation of these receptors across both models. These data support interpretation of intracellular HSA measurements, but do not establish receptor-mediated uptake. Together, these findings support the suitability of albumin as a versatile carrier scaffold while underscoring that nanoparticle internalization is governed by cell-type–specific factors rather than a uniform receptor-dependent process.[56]

Retinal neurodegenerative disorders represent one of the most immediate translational contexts for neurotrophin-based therapies.[57–59] Inherited conditions such as Stargardt disease and retinitis pigmentosa, as well as acquired pathologies including age-related macular degeneration (AMD), involve progressive degeneration of retinal neurons and supporting cells, making them attractive targets for neuroprotective strategies.[58] Importantly, intravitreal administration enables direct access to retinal tissue, which is developmentally and functionally part of the central nervous system, thereby bypassing the need to overcome the blood–brain barrier. While the present study focuses on local delivery and early biological responses, the developed PEGylated albumin-based platform can be considered in a broader context of nervous system–oriented applications, where the therapeutic potential of neurotrophins is widely recognized but remains challenging to harness. A central question in this context concerns the ability of albumin to access the brain. Although native albumin exhibits limited permeability across the intact blood–brain barrier (BBB), substantial evidence indicates that BBB integrity is frequently compromised in neurodegenerative conditions, potentially increasing access of circulating proteins to the central nervous system.[60–62] In parallel, independent studies have demonstrated that nano-formulated HSA can engage specific transport or transcytotic pathways at the BBB, including gp60/SPARC-associated mechanisms or receptor-targeted strategies engineered at the nanoparticle surface.[63–68] Alternative delivery routes, such as intranasal administration, further support the feasibility of albumin-based systems to reach defined brain regions while limiting systemic exposure.[69–71] These considerations provide a rationale for continued exploration of albumin-based nanocarriers as adaptable delivery platforms for neurological, in line with ongoing research in neurodegeneration that increasingly emphasizes nanomaterials targeting neuroinflammation, particularly in Alzheimer's disease.[72] From a robustness perspective, neurodegenerative environments are characterized by oxidative stress, altered protein homeostasis, and heightened cellular vulnerability, placing stringent demands on delivery systems. Albumin possesses intrinsic antioxidative properties,[73] and, as demonstrated in this study, PEGylated albumin-based nanoparticles preserve cargo functionality and support cellular resilience under oxidative stress conditions. Together, these attributes justify further platform-oriented development and targeted investigation in future, disease-specific models.

Conclusion

This study demonstrates that PEGylated human serum albumin nanoparticles enable stable and efficient intracellular delivery of BDNF and NT3 across complementary experimental systems. The platform maintains physicochemical stability, supports neurotrophin adsorption without loss of colloidal integrity, and ensures carrier internalization in human epithelial and neuronal cells.

Following intraocular administration in the rabbit eye, the nanoparticles exhibited transient BDNF detectability and exploratory transcriptional changes without a coordinated pro-apoptotic response under the tested conditions. These preliminary findings are consistent with biological compatibility in a second species but require further validation in adequately powered in vivo studies. The limited sample size and absence of formal inferential statistics in the rabbit study restrict conclusions regarding in vivo safety and biological compatibility. Therefore, these data should be interpreted as exploratory

and hypothesis-generating. In human cell models exposed to oxidative stress, nanoparticle-mediated delivery resulted in robust intracellular accumulation of neurotrophins, attenuation of lipid peroxidation, reduced apoptosis-associated cell populations, and transcript-level changes consistent with preserved biological activity of the delivered neurotrophins.

Together, these findings show that PEGylated albumin nanoparticles function as a robust protein delivery platform capable of maintaining cargo functionality under biologically challenging conditions. The data provide a clear experimental basis for further development of albumin-based nanocarriers for applications where oxidative stress and limited protein stability represent critical barriers.

Abbreviations

6-OHDA, 6-Hydroxydopamine; AFM, Atomic Force Microscopy; BDNF, Brain-Derived Neurotrophic Factor; CNKSR2, Connector Enhancer of Kinase Suppressor of Ras 2; CREB, cAMP Response Element-Binding Protein; CREBBP (CBP), CREB-Binding Protein; DLS, Dynamic Light Scattering; ELS, Electrophoretic Light Scattering; HSA, Human Serum Albumin; MADLS, Multi-Angle Dynamic Light Scattering; MAPK, Mitogen-Activated Protein Kinase; MAPK1, Mitogen-Activated Protein Kinase 1 (ERK2); MAPKAPK2, MAPK-Activated Protein Kinase 2; MAPKAPK3, MAPK-Activated Protein Kinase 3; MKNK1, MAPK-Interacting Serine/Threonine-Protein Kinase 1; $NaIO_3$ - Sodium Iodate; NF-κB, Nuclear Factor kappa B; NP - Nanoparticle; NT3, Neurotrophin-3; NTRK2, Neurotrophic Receptor Tyrosine Kinase 2 (TrkB); NTRK3, Neurotrophic Receptor Tyrosine Kinase 3 (TrkC); PDI, Polidispersity Index; Pcna, Proliferating Cell Nuclear Antigen; PEG, Poly (ethylene glycol); qPCR, Quantitative Polymerase Chain Reaction; Ras, Rat Sarcoma GTPase; TrkB, Tropomyosin Receptor Kinase B; TrkC, Tropomyosin Receptor Kinase C.

Artificial Intelligence Tool Disclosure

ChatGPT (OpenAI, GPT-4/GPT-5 models) was used to assist with language editing, including grammar correction, stylistic improvements, and typo elimination, and with the iterative development of a conceptual workflow illustration presented as Figure 1. The AI tool was used exclusively for editorial and illustrative support purposes and not for the generation, analysis, or interpretation of scientific data. All AI-assisted text and visual content were reviewed, refined, and verified by the authors to ensure originality, accuracy, and consistency with the intended scientific meaning. The authors take full responsibility for the integrity of the final content, including the accuracy of references and the conceptual workflow illustration. The authors have reviewed the terms of use of the AI tool and confirm that the generated content is suitable for publication. The authors further confirm that they hold the rights necessary for publication of the generated visual material.

Data Sharing Statement

The dataset(s) supporting the conclusions of this article is(are) available upon request from the relevant corresponding author: physicochemical characterization data from Maria Dabkowska (maria.dabkowska@pum.edu.pl) and in vitro/in vivo data from Iga Stukan (iga.stukan@pum.edu.pl).

Author Contributions

Conceptualization: IS, MD, BM; In vitro studies: IS, MD, KP, MW, PS; In vivo studies: AM, KŁ, MW, DW, JZ, BK, MSz, IB, IS, MD; Statistical analysis: IS, MD; Funding acquisition: BM; Supervision: BM; Writing – original draft: IS, MD; Writing – review & editing: IS, MD, AM, MK, BM. All authors reviewed the manuscript and declared no competing interests. All authors made a significant contribution to the work reported, whether that is in the conception, study design, execution, acquisition of data, analysis and interpretation, or in all these areas; took part in drafting, revising or critically reviewing the article; gave final approval of the version to be published; have agreed on the journal to which the article has been submitted; and agree to be accountable for all aspects of the work.

Funding

This work was supported by European Union funds from the European Union Regional Development Fund, Interreg Cooperation Program VI A Mecklenburg-Western Pomerania / Brandenburg / Poland for 2021–2027: No INT0100010; and also by the Medical Research Agency (Agencja Badań Medycznych), NeOStem 2020/ABM/01/00014 "Innovative

use of stem cells and biocompatible polyelectrolyte nanoparticles releasing neurotrophins in the adjuvant treatment of neurodegenerative diseases".

Disclosure

On October 10th, 2023, a patent application was filed in Poland under the number P.446343. The patent is entitled "The pharmaceutical composition for intravitreal administration containing at least one active substance and a carrier, electrostatic complex containing at least one active substance and a carrier, and its application". This patent is based on a method for producing nanoparticles used in this work. The inventors of this patent are Maria Dąbkowska, Bogusław Machaliński, Iga Stukan, and Alicja Kosiorowska. Dr Maria Dąbkowska reports grants from European Union Regional Development Fund, Interreg Cooperation Program VI A Mecklenburg-Western Pomerania / Brandenburg / Poland for 2021–2027: No INT0100010; and also by the Medical Research Agency (Agencja Badań Medycznych), NeOStem 2020/ABM/01/00014 "Innovative use of stem cells and biocompatible polyelectrolyte nanoparticles releasing neurotrophins in the adjuvant treatment of neurodegenerative diseases", outside the submitted work. Mrs Kamila Pukacka reports grants from European Union Regional Development Fund, Interreg Cooperation Program VI A Mecklenburg-Western Pomerania / 797 Brandenburg / Poland for 2021–2027: No INT0100010; and also by the Medical Research Agency (Agencja Badań Medycznych), NeOStem 2020/ABM/01/00014 "Innovative use of stem cells and biocompatible polyelectrolyte nanoparticles releasing neurotrophins in the adjuvant treatment of neurodegenerative diseases", outside the submitted work; In addition, Mrs Kamila Pukacka has a patent The Patent Office of the Republic of Poland pending to P.446343.

The authors report no other conflicts of interest in this work.

References

1. Palasz E, Wysocka A, Gasiorowska A, Chalimoniuk M, Niewiadomski W, Niewiadomska G. BDNF as a promising therapeutic agent in parkinson's disease. *IJMS*. 2020;21(3):1170. doi:10.3390/ijms21031170
2. Inanc Tekin M, Sekeroglu MA, Demirtas C, et al. Brain-derived neurotrophic factor in patients with age-related macular degeneration and its correlation with retinal layer thicknesses. *Invest Ophthalmol Vis Sci*. 2018;59(7):2833–2840. doi:10.1167/iovs.18-24030
3. Miranda-Lourenço C, Ribeiro-Rodrigues L, Fonseca-Gomes J, et al. Challenges of BDNF-based therapies: from common to rare diseases. *Pharmacolog Res*. 2020;162:105281. doi:10.1016/j.phrs.2020.105281
4. Nagahara AH, Tuszynski MH. Potential therapeutic uses of BDNF in neurological and psychiatric disorders. *Nat Rev Drug Discov*. 2011;10 (3):209–219. doi:10.1038/nrd3366
5. Amidfar M, de Oliveira J, Kucharska E, Budni J, Kim YK. The role of CREB and BDNF in neurobiology and treatment of Alzheimer's disease. *Life Sci*. 2020;257:118020. doi:10.1016/j.lfs.2020.118020
6. Arora S, Kanekiyo T, Singh J. Functionalized nanoparticles for brain targeted BDNF gene therapy to rescue Alzheimer's disease pathology in transgenic mouse model. *Int J Biol Macromol*. 2022;208:901–911. doi:10.1016/j.ijbiomac.2022.03.203
7. Zhou X, Deng X, Liu M, et al. Intranasal delivery of BDNF-loaded small extracellular vesicles for cerebral ischemia therapy. *J Controlled Release*. 2023;357:1–19. doi:10.1016/j.jconrel.2023.03.033
8. Cang MX, Liu P, ling ZX, et al. Intranasal delivery of recombinant AAV containing BDNF fused with HA2TAT: a potential promising therapy strategy for major depressive disorder. *Sci Rep*. 2016;6(1):22404. doi:10.1038/srep22404
9. Mattern L, Otten K, Miskey C, et al. Molecular and functional characterization of BDNF-overexpressing human retinal pigment epithelial cells established by sleeping beauty transposon-mediated gene transfer. *Int J Mol Sci*. 2022;23(21):12982. doi:10.3390/ijms232112982
10. Jiang Y, Fay JM, Poon C, et al. Nanoformulation of brain-derived neurotrophic factor with target receptor-triggered-release in the central nervous system. *Adv Funct Mat*. 2018;28(6):1703982. doi:10.1002/adfm.201703982
11. Shen Y, Li N, Sun S, et al. Non-invasive, targeted, and non-viral ultrasound-mediated brain-derived neurotrophic factor plasmid delivery for treatment of autism in a rat model. *Front Neurosci*. 2022;16:986571. doi:10.3389/fnins.2022.986571
12. Koennings S, Sapin A, Blunk T, Menei P, Goepferich A. Towards controlled release of BDNF — manufacturing strategies for protein-loaded lipid implants and biocompatibility evaluation in the brain. *J Controlled Release*. 2007;119(2):163–172. doi:10.1016/j.jconrel.2007.02.005
13. Budenz CL, Wong HT, Swiderski DL, Shibata SB, Pfingst BE, Raphael Y. Differential effects of AAV.BDNF and AAV.Ntf3 in the deafened adult Guinea pig ear. *Sci Rep*. 2015;5:8619. doi:10.1038/srep08619
14. St Peter M, Brough DE, Lawrence A, et al. Improving control of gene therapy-based neurotrophin delivery for inner ear applications. *Front Bioeng Biotechnol*. 2022;10:892969. doi:10.3389/fbioe.2022.892969
15. Rabbani G, Ahn SN. Structure, enzymatic activities, glycation and therapeutic potential of human serum albumin: a natural cargo. *Int J Biol Macromol*. 2019;123:979–990. doi:10.1016/j.ijbiomac.2018.11.053
16. Dąbkowska M, Stukan I, Kosiorowska A, et al. In vitro and in vivo characterization of human serum albumin-based PEGylated nanoparticles for BDNF and NT3 codelivery. *Int J Biol Macromol*. 2024;265:130726. doi:10.1016/j.ijbiomac.2024.130726
17. Stukan I, Żuk A, Pukacka K, et al. Wolf in sheep's clothing: taming cancer's resistance with human serum albumin? *IJN*. 2025;20:3493–3525. doi:10.2147/IJN.S500997
18. Mariam J, Sivakami S, Dongre PM. Albumin Corona on nanoparticles – a strategic approach in drug delivery. *Drug Delivery*. 2016;23 (8):2668–2676. doi:10.3109/10717544.2015.1048488

19. Dąbkowska M, Kosiorowska-Kraj A, Szatanik A, et al. Tunable PEGylated albumin nanocarriers enhance 5-FU cytotoxic selectivity and modulate oxidative and immune stress in colorectal cancer model. *Biomed Pharmacother*. 2026;196:118958. doi:10.1016/j.biopha.2025.118958
20. Danhier F, Ansorena E, Silva JM, Coco R, Le Breton A, Préat V. PLGA-based nanoparticles: an overview of biomedical applications. *J Controlled Release*. 2012;161(2):505–522. doi:10.1016/j.jconrel.2012.01.043
21. Sercombe L, Veerati T, Moheimani F, Wu SY, Sood AK, Hua S. Advances and challenges of liposome assisted drug delivery. *Front Pharmacol*. 2015. doi:10.3389/fphar.2015.00286
22. Larsen MT, Kuhlmann M, Hvam ML, Howard KA. Albumin-based drug delivery: harnessing nature to cure disease. *Mol Cell Ther*. 2016;4(1):3. doi:10.1186/s40591-016-0048-8
23. Liu B, Wang W, Shah A, et al. Sodium iodate induces ferroptosis in human retinal pigment epithelium ARPE-19 cells. *Cell Death Dis*. 2021;12 (3):230. doi:10.1038/s41419-021-03520-2
24. Zhang XY, Ng TK, Brelén ME, et al. Continuous exposure to non-lethal doses of sodium iodate induces retinal pigment epithelial cell dysfunction. *Sci Rep*. 2016;6(1):37279. doi:10.1038/srep37279
25. Xicoy H, Wieringa B, Martens GJM. The SH-SY5Y cell line in Parkinson's disease research: a systematic review. *Mol Neurodegen*. 2017;12(1):10. doi:10.1186/s13024-017-0149-0
26. Lopes FM, Schröder R, MLCDF J, et al. Comparison between proliferative and neuron-like SH-SY5Y cells as an in vitro model for Parkinson disease studies. *Brain Res*. 2010;1337:85–94. doi:10.1016/j.brainres.2010.03.102
27. Dąbkowska M, Kosiorowska A, Machaliński B. The impact of serum protein adsorption on PEGylated NT3–BDNF nanoparticles—distribution, protein release, and cytotoxicity in a human retinal pigmented epithelial cell model. *Pharmaceutics*. 2023;15(9):2236. doi:10.3390/pharmaceutics15092236
28. Dąbkowska M, Adamczyk Z, Cieśla M, Adamczak M, Bober J. Lysozyme monolayers at polymer microparticles: electrokinetic characteristics and modeling. *J Phys Chem C*. 2018;122(31):17846–17855. doi:10.1021/acs.jpcc.8b04916
29. Dąbkowska M, Ulańczyk Z, Łuczkowska K, et al. The role of the electrokinetic charge of neurotrophis-based nanocarriers: protein distribution, toxicity, and oxidative stress in in vitro setting. *J Nanobiotechnol*. 2021;19(1):258. doi:10.1186/s12951-021-00984-4
30. Wasilewska M, Adamczyk Z, Jachimska B. Structure of fibrinogen in electrolyte solutions derived from dynamic light scattering (DLS) and viscosity measurements. *Langmuir*. 2009;25(6):3698–3704. doi:10.1021/la803662a
31. Adamczyk Z, Nattich M, Wasilewska M, Zaucha M. Colloid particle and protein deposition - electrokinetic studies. *Adv Colloid Interface Sci*. 2011;168(1–2):3–28. doi:10.1016/j.cis.2011.04.002
32. Zhang T, Gygi SP, Paulo JA. Temporal proteomic profiling of SH-SY5Y differentiation with retinoic acid using FAIMS and real-time searching. *J Proteome Res*. 2021;20(1):704–714. doi:10.1021/acs.jproteome.0c00614
33. Targett IL, Crompton LA, Conway ME, Craig TJ. Differentiation of SH-SY5Y neuroblastoma cells using retinoic acid and BDNF: a model for neuronal and synaptic differentiation in neurodegeneration. *In Vitro Cell Dev Biol–Animal*. 2024;60(9):1058–1067. doi:10.1007/s11626-024-00948-6
34. Keefe K, Sheikh I, Smith G. Targeting neurotrophins to specific populations of neurons: NGF, BDNF, and NT-3 and their relevance for treatment of spinal cord injury. *IJMS*. 2017;18(3):548. doi:10.3390/ijms18030548
35. Suk JS, Xu Q, Kim N, Hanes J, Ensign LM. PEGylation as a strategy for improving nanoparticle-based drug and gene delivery. *Adv Drug Delivery Rev*. 2016;99:28–51. doi:10.1016/j.addr.2015.09.012
36. Owensiii D, Peppas N. Opsonization, biodistribution, and pharmacokinetics of polymeric nanoparticles. *Int J Pharmaceut*. 2006;307(1):93–102. doi:10.1016/j.ijpharm.2005.10.010
37. He C, Hu Y, Yin L, Tang C, Yin C. Effects of particle size and surface charge on cellular uptake and biodistribution of polymeric nanoparticles. *Biomaterials*. 2010;31(13):3657–3666. doi:10.1016/j.biomaterials.2010.01.065
38. Reflection Paper on Nanotechnology-Based Medicinal Products for Human Use. European Medicines Agency; 2011. Available from: https://www.ema.europa.eu/en/documents/regulatory-procedural-guideline/reflection-paper-nanotechnology-based-medicinal-products-human-use_en.pdf. Accessed June 16, 2026.
39. Sofińska K, Adamczyk Z, Kujda M, Nattich-Rak M. Recombinant albumin monolayers on latex particles. *Langmuir*. 2014;30(1):250–258. doi:10.1021/la403715s
40. Dąbkowska M, Rogińska D, Kłos P, et al. Electrostatic complex of neurotrophin 4 with dendrimer nanoparticles: controlled release of protein in vitro and in vivo. *IJN*. 2019;14:6117–6131. doi:10.2147/IJN.S210140
41. Dąbkowska M, Adamczyk Z. Human serum albumin monolayers on mica: electrokinetic characteristics. *Langmuir*. 2012;28(44):15663–15673. doi:10.1021/la3036677
42. Prozeller D, Rosenauer C, Morsbach S, Landfester K. Immunoglobulins on the surface of differently charged polymer nanoparticles. *Biointerphases*. 2020;15(3):031009. doi:10.1116/6.0000139
43. Hamidi M, Azadi A, Rafiei P. Pharmacokinetic consequences of pegylation. *Drug Delivery*. 2006;13(6):399–409. doi:10.1080/10717540600814402
44. Maisonpierre PC, Le Beau MM, Espinosa R, et al. Human and rat brain-derived neurotrophic factor and neurotrophin-3: gene structures, distributions, and chromosomal localizations. *Genomics*. 1991;10(3):558–568. doi:10.1016/0888-7543(91)90436-I
45. Kaplan DR, Miller FD. Neurotrophin signal transduction in the nervous system. *Current Opinion Neurobiol*. 2000;10(3):381–391. doi:10.1016/S0959-4388(00)00092-1
46. ElShamy WM, Ernfors PB-DNF. Neurotrophin-3, and neurotrophin-4 complement and cooperate with each other sequentially during visceral neuron development. *J Neurosci*. 1997;17(22):8667–8675. doi:10.1523/JNEUROSCI.17-22-08667.1997
47. Brock JH, Rosenzweig ES, Blesch A, et al. Local and remote growth factor effects after primate spinal cord injury. *J Neurosci*. 2010;30 (29):9728–9737. doi:10.1523/JNEUROSCI.1924-10.2010
48. Tan J, Wang Y, Yip X, Glynn F, Shepherd RK, Caruso F. Nanoporous peptide particles for encapsulating and releasing neurotrophic factors in an animal model of neurodegeneration. *Adv Mater*. 2012;24(25):3362–3366. doi:10.1002/adma.201200634
49. Del Rio D, Stewart AJ, Pellegrini N. A review of recent studies on malondialdehyde as toxic molecule and biological marker of oxidative stress. *Nutr Metab Cardiovasc Dis*. 2005;15(4):316–328. doi:10.1016/j.numecd.2005.05.003
50. Dąbkowska M, Stukan I, Kowalski B, et al. BDNF-loaded PDADMAC-heparin multilayers: a novel approach for neuroblastoma cell study. *Sci Rep*. 2023;13(1):17939. doi:10.1038/s41598-023-45045-y
51. Kim J, Bronson CL, Hayton WL, et al. Albumin turnover: fcRn-mediated recycling saves as much albumin from degradation as the liver produces. *Am J Physiol Gastrointest Liver Physiol*. 2006;290(2):G352–360. doi:10.1152/ajpgi.00286.2005

52. Nakamura K, Yamanouchi K, Nishihara M. Secreted protein acidic and rich in cysteine internalization and its age-related alterations in skeletal muscle progenitor cells. *Aging Cell*. 2014;13(1):175–184. doi:10.1111/acel.12168
53. Hoang B, Ernsting MJ, Roy A, Murakami M, Undzys E, Li SD. Docetaxel-carboxymethylcellulose nanoparticles target cells via a SPARC and albumin dependent mechanism. *Biomaterials*. 2015;59:66–76. doi:10.1016/j.biomaterials.2015.04.032
54. Schirò G, Iacono S, Ragonese P, Aridon P, Salemi G, Balistreri CR. A brief overview on BDNF-Trk pathway in the nervous system: a potential biomarker or possible target in treatment of multiple sclerosis? *Front Neurol*. 2022;13:917527. doi:10.3389/fneur.2022.917527
55. Kolarow R, Brigadski T, Lessmann V. Postsynaptic secretion of BDNF and NT-3 from hippocampal neurons depends on Calcium–Calmodulin Kinase II signaling and proceeds via delayed fusion pore opening. *J Neurosci*. 2007;27(39):10350–10364. doi:10.1523/JNEUROSCI.0692-07.2007
56. Recouvreux MV, Commisso C. Macropinocytosis: a metabolic adaptation to nutrient stress in cancer. *Front Endocrinol*. 2017;8:261. doi:10.3389/fendo.2017.00261
57. Pardue MT, Allen RS. Neuroprotective strategies for retinal disease. *Prog Retin Eye Res*. 2018;65:50–76. doi:10.1016/j.preteyeres.2018.02.002
58. Blouin L, Sahel JA, Chung DC. Neurotrophic factors in the treatment of inherited retinal diseases. *Cold Spring Harb Perspect Med*. 2024;14(12):a041665. doi:10.1101/cshperspect.a041665
59. Daly C, Ward R, Reynolds AL, Galvin O, Collery RF, Kennedy BN. Brain-Derived Neurotrophic Factor as a Treatment Option for Retinal Degeneration. In: Ash JD, Anderson RE, LaVail MM, Bowes Rickman C, Hollyfield JG, Grimm C editors. *Retinal Degenerative Diseases. Vol 1074. Advances in Experimental Medicine and Biology*. Springer International Publishing; 2018:465–471. doi:10.1007/978-3-319-75402-4_57.
60. Saraiva C, Praça C, Ferreira R, Santos T, Ferreira L, Bernardino L. Nanoparticle-mediated brain drug delivery: overcoming blood-brain barrier to treat neurodegenerative diseases. *J Control Release*. 2016;235:34–47. doi:10.1016/j.jconrel.2016.05.044
61. LeVine SM. Albumin and multiple sclerosis. *BMC Neurol*. 2016;16:47. doi:10.1186/s12883-016-0564-9
62. Assialioui A, Domínguez R, Ferrer I, Andrés-Benito P, Povedano M. Elevated cerebrospinal fluid proteins and albumin determine a poor prognosis for spinal amyotrophic lateral sclerosis. *Int J Mol Sci*. 2022;23(19):11063. doi:10.3390/ijms231911063
63. Lin T, Zhao P, Jiang Y, et al. Blood–brain-barrier-penetrating albumin nanoparticles for biomimetic drug delivery via albumin-binding protein pathways for antiglioma therapy. *ACS Nano*. 2016;10(11):9999–10012. doi:10.1021/acsnano.6b04268
64. Shastri D, Raj V, Lee S. Revolutionizing Alzheimer's treatment: harnessing human serum albumin for targeted drug delivery and therapy advancements. *Ageing Res Rev*. 2024;99:102379. doi:10.1016/j.arr.2024.102379
65. Perumal V, Ravula AR, Agas A, et al. Transferrin-grafted albumin nanoparticles for the targeted delivery of apocynin and neuroprotection in an in vitro model of the BBB. *Micro*. 2023;3(1):84–106. doi:10.3390/micro3010008
66. Muniswamy VJ, Raval N, Gondaliya P, Tambe V, Kalia K, Tekade RK. "Dendrimer-Cationized-Albumin" encrusted polymeric nanoparticle improves BBB penetration and anticancer activity of doxorubicin. *Int J Pharm*. 2019;555:77–99. doi:10.1016/j.ijpharm.2018.11.035
67. Ruan C, Liu L, Lu Y, et al. Substance P-modified human serum albumin nanoparticles loaded with paclitaxel for targeted therapy of glioma. *Acta Pharm Sin B*. 2018;8(1):85–96. doi:10.1016/j.apsb.2017.09.008
68. Koga T, Kida H, Yamasaki Y, et al. Intracranial gene delivery mediated by albumin-based nanobubbles and low-frequency ultrasound. *Nanomaterials*. 2024;14(3):285. doi:10.3390/nano14030285
69. Meredith ME, Salameh TS, Banks WA. Intranasal delivery of proteins and peptides in the treatment of neurodegenerative diseases. *AAPS J*. 2015;17(4):780–787. doi:10.1208/s12248-015-9719-7
70. Migliore MM, Vyas TK, Campbell RB, Amiji MM, Waszczak BL. Brain delivery of proteins by the intranasal route of administration: a comparison of cationic liposomes versus aqueous solution formulations. *J Pharm Sci*. 2010;99(4):1745–1761. doi:10.1002/jps.21939
71. Falcone JA, Salameh TS, Yi X, et al. Intranasal administration as a route for drug delivery to the brain: evidence for a unique pathway for albumin. *J Pharmacol Exp Ther*. 2014;351(1):54–60. doi:10.1124/jpet.114.216705
72. Hong X, Chen T, Liu Y, et al. Design, current states, and challenges of nanomaterials in anti-neuroinflammation: a perspective on Alzheimer's disease. *Ageing Res Rev*. 2025;105:102669. doi:10.1016/j.arr.2025.102669
73. Roche M, Rondeau P, Singh NR, Tarnus E, Bourdon E. The antioxidant properties of serum albumin. *FEBS Lett*. 2008;582(13):13. doi:10.1016/j.febslet.2008.04.057